Modeling extreme events and intermittency in turbulent diffusion with a mean gradient

Mustafa A. Mohamad*[1] and Di Qi†[2]

[1]Department of Mechanical and Manufacturing Engineering, University of Calgary, Calgary, AB, Canada
[2]Department of Mathematics, Purdue University, West Lafayette, IN, USA

May 17, 2025

Abstract

We study the statistical properties of passive tracer transport in turbulent flows with a mean gradient, emphasizing tracer intermittency and extreme events. An analytically tractable model is developed, coupling zonal and shear velocity components with both linear and nonlinear stochastic dynamics. Formulating the model in Fourier space, a simple explicit solution for the tracer invariant statistics is derived. Through this model we identify the resonance condition responsible for non-Gaussian behavior and bursts in the tracer field. Resonant conditions, that lead to a peak in the tracer variance, occur when the zonal flow and the shear flow phase speeds are equivalent. Numerical experiments across a range of regimes, including different energy spectra and zonal flow models, are performed to validate these findings and demonstrate how the velocity field and stochasticity determines tracer bursts. These results provide additional insight into the mechanisms underlying turbulent tracer transport, with implications for uncertainty quantification and data assimilation in geophysical and environmental applications.

1 Introduction

Turbulent transport of passive scalars represents a fundamental phenomenon in fluid dynamics. The physical law that describes the transport of a passive scalar $T_t(\boldsymbol{x})$ (subscript denotes time dependence) is given by the advection-diffusion equation:

$$\frac{\partial T_t}{\partial t} + \boldsymbol{v}_t \cdot \nabla T_t = \kappa \Delta T_t + S_t(\boldsymbol{x}), \qquad T_{t=0}(\boldsymbol{x}) = T_0(\boldsymbol{x}) \tag{1}$$

where $\kappa > 0$ is the molecular diffusivity constant, $\boldsymbol{v}_t$ is an incompressible velocity field satisfying $\nabla \cdot \boldsymbol{v}_t = 0$, and $S_t(\boldsymbol{x})$ is a source term.

Passive tracers include physical tracers such as temperature, and chemical tracers, including solute tracer burst. These tracers play a crucial role as diagnostic tools in environmental and geophysical sciences. While the advection-diffusion equation and turbulent mixing of passive scalars has been extensively studied since the works of Taylor [15], Richardson [13], and Kolmogorov [4] among many others, understanding the statistical properties of tracer fields, particularly their intermittent behavior, remains an active area of interest [14, 17].

In this article, we focus on the statistical aspects of the tracer field, with particular emphasis on tracer intermittency and extreme events. These phenomena have significant consequences in practical applications including: the spread of pollutants and hazardous chemicals in the air and atmosphere (such as sulfur dioxide), the dispersion of anthropogenic contaminants in water bodies, and the behavior of Lagrangian tracers like measurement floats in the ocean that collect environmental data [12]. Through analytical models and simulation, we study the effects of intermittency for different velocity models and provide intuition on the physical features of corresponding tracer fields.

The model developed here extends and builds upon an existing line of literature from whereby elementary models for turbulent diffusion are constructed starting from various simplified assumptions on the underlying velocity field. These works starting from deterministic models of time-dependent fields [11] and periodic shear flows [1], to more recent works

*Corresponding author. Email: mustafa.mohamad@ucalgary.ca
†Email: qidi@purdue.edu

where more realistic stochastic representations have been assumed [7]. In between, various models have been studies, from models with uncorrelated velocity fields, to white noise limits of the shear flow, to studies of eddy-diffusivity approximations of these models [9]. A comprehensive review on the literature on passive scalar transport and various approximations is provided in the work by Majda and Kramer [10].

The paper is organized as follows: After introducing our key contributions in section 1.1, in section 2 we present a detailed formulation of turbulent diffusion models with a mean gradient. Section 3 examines the general properties of these models, followed by section 4 which examines their statistical solutions. Section 4.2 provides the resonance conditions and discusses their physical interpretation. In sections 5 and 6, we present numerical results demonstrating various intermittency regimes, and we conclude with a discussion of implications and future directions in section 8.

1.1 Contributions

Contributions in this paper include an analytically tractable model to study tracer intermittency, explicit tracer statistical solutions showing extreme events, and extensive numerical simulations displaying intermittency in different model regimes. We show a range of tracer intermittency scenarios that can be used for various studies in uncertainty quantification (UQ) and data assimilation (DA) applications.

2 Formulation of turbulent diffusion models with a mean gradient

In general, the transport of a passive tracer $T_t(\boldsymbol{x})$ advected by an incompressible velocity field $\boldsymbol{v}_t(\boldsymbol{x})$ is given by

$$\frac{\partial T_t}{\partial t} + \boldsymbol{v}_t \cdot \nabla T_t = \kappa \Delta T_t + S_t(\boldsymbol{x}), \qquad \nabla \cdot \boldsymbol{v}_t = 0, \tag{2}$$

where κ is molecular diffusivity and $S_t(\boldsymbol{x})$ a tracer external source term. We study two-dimensional turbulent diffusion models where the passive tracer field has a known background mean gradient $\boldsymbol{\alpha} = (\alpha_x, \alpha_y)$, so that the tracer field can be written as

$$T_t(\boldsymbol{x}) = \boldsymbol{\alpha} \cdot \boldsymbol{x} + T_t'(\boldsymbol{x}), \tag{3}$$

where the prime notation denotes fluctuations of the tracer field around the mean gradient term.

In the model we consider, the stochastic velocity field $\boldsymbol{v}_t$ is periodic in space with the form

$$\boldsymbol{v}_t(x) = (u_t, v_t(x)), \tag{4}$$

which automatically satisfies the incompressibility condition. The spatially uniform horizontal velocity u_t represents zonal cross sweeps, such as east-west zonal jets, and $v_t(x)$ is a shear flow along the y-axis, representing transverse waves, such as north-south Rossby waves. The equation for the tracer fluctuation term T' using eq. (2) is then given by

$$\frac{\partial T_t'}{\partial t} + u_t \frac{\partial T_t'}{\partial x} + v_t(x) \frac{\partial T_t'}{\partial y} = \kappa \Delta T_t' - \alpha_x u_t - \alpha_y v_t(x) + S_t(\boldsymbol{x}). \tag{5}$$

For the simplified test model, we consider the existence of a background mean gradient in the vertical direction, thus $\alpha_x \equiv 0$. Further, motivated from physical considerations, we consider fluctuations that only depend on the x variable alone so that

$$T_t(x, y) = T_t'(x) + \alpha y, \tag{6}$$

where we redefine $\alpha \equiv \alpha_y$. The fluctuations then satisfy the simplified model

$$\frac{\partial T_t}{\partial t} + u_t \frac{\partial T_t}{\partial x} = \kappa \frac{\partial^2 T_t}{\partial x^2} - d_T T_t - \alpha v_t(x), \tag{7}$$

where we drop the prime notation from T' and source terms $S_t(\boldsymbol{x}) \equiv 0$. The term with $d_T > 0$ is an explicit uniform damping term added to damp the zero mode that arises from partial Fourier transform in the y variable at non-zero modes in the general model in eq. (5). This explicit damping term compensates for the lack of natural damping in the zero mode due to the absence of spatial y derivatives in the simplified model [10].

We see that in eq. (7) the random velocity $v_t(x)$ drives fluctuations in the tracer field through the mean gradient α. These judicious simplifications preserve key features of various inertial range statistics in turbulent diffusion, including intermittency, while yielding analytically tractable tracer solutions that facilitate rigorous mathematical analysis [9].

2.1 Velocity field and passive tracer model in Fourier space

Next we formulate the velocity field for the passively advected tracer. We chose a general stochastic representation in order to capture the range of patterns that appear in general turbulent signals. There are two components to the velocity field $\boldsymbol{v}_t = (u_t, v_t(x))$, a zonal component u_t and a spatially dependent shear term $v_t(x)$.

The spatially uniform zonal flow, i.e. the cross sweep, satisfies the nonlinear stochastic diffusion equation:

$$du_t = f(u_t)\,dt + \sigma(u_t)\,dW_t, \tag{8}$$

where W_t is a real Wiener process. The velocity u_t can be decomposed into

$$u_t = \overline{u} + u_t', \tag{9}$$

consisting of an ensemble mean $\overline{u}$ and a fluctuating component u_t'.

The shear velocity $v_t(x)$ satisfies a stochastic partial differential equation of the form

$$\frac{\partial v_t}{\partial t} + P\left(\frac{\partial}{\partial x}, u_t\right)v_t = \dot{W}_v(x,t), \tag{10}$$

where P is a linear operator that combines both dispersive and dissipative effects acting on v_t, coupled with the zonal flow u_t. The spatially dependent shear flow $v_t(x)$ is modeled by the following stochastically forced dissipative advection PDE, where the cross sweep dependence u_t enters linearly,

$$\frac{\partial v_t}{\partial t} = u_t R_1\left(\frac{\partial}{\partial x}\right)v_t + R_2\left(\frac{\partial}{\partial x}\right)v_t - \gamma_v\left(\frac{\partial}{\partial x}\right)v_t + \dot{W}_v(x,t). \tag{11}$$

Here the linear operators R_1, R_2, γ_v are defined through their image on Fourier modes:

$$R_1\left(\frac{\partial}{\partial x}\right) = ia_k e^{ikx}, \qquad R_2\left(\frac{\partial}{\partial x}\right) = ib_k e^{ikx}, \qquad \gamma_v\left(\frac{\partial}{\partial x}\right) = \gamma_{v,k} e^{ikx}, \tag{12}$$

such that γ_v is a positive definite linear operator $\gamma_{v,k} > 0$ representing dissipation, and R_1, R_2 are linear operators that represent both internal effects of u_t on v_t and wavelike effects, respectively, so that the real-valued dispersion relation is given by:

$$\omega_{v,k} = a_k u_t + b_k. \tag{13}$$

With the above description a summary of the simplified turbulent diffusion model in physical space is given by

$$du_t = f(u_t)\,dt + \sigma(u_t)\,dW_t, \tag{14}$$

$$\frac{\partial v_t}{\partial t} = u_t R_1\left(\frac{\partial}{\partial x}\right)v_t + R_2\left(\frac{\partial}{\partial x}\right)v_t - \gamma_v\left(\frac{\partial}{\partial x}\right)v_t + \dot{W}_v(x,t), \tag{15}$$

$$\frac{\partial T_t}{\partial t} = -u_t\frac{\partial T_t}{\partial x} - d_T T_t + \kappa\frac{\partial^2 T_t}{\partial x^2} - \alpha v_t. \tag{16}$$

Note that since the equations for v_t and T_t are linear, we employ the following Fourier expansion (the conjugating Fourier modes ensure $T_t(x) \in \mathbb{R}$ and $v_t(x) \in \mathbb{R}$)

$$T_t(x) = \sum_k \widehat{T}_{k,t} e^{ikx}, \quad \widehat{T}_{-k,t} = \widehat{T}^*_{k,t}, \quad \text{and} \quad v_t(x) = \sum_k \hat{v}_{k,t} e^{ikx}, \quad \hat{v}_{-k,t} = \hat{v}^*_{k,t}, \tag{17}$$

to write the explicit equation for each wavenumber to write the model in Fourier space.

Definition 2.1. *The turbulent shear model in Fourier space can be formulated as*

$$du_t = f(u_t)\,dt + \sigma(u_t)\,dW_t, \tag{18}$$

$$d\hat{v}_{k,t} = (-\gamma_{v,k} + i\omega_{v,k})\hat{v}_{k,t}\,dt + \sigma_{v,k}\,dB_{k,t}, \tag{19}$$

$$d\widehat{T}_{k,t} = (-\gamma_{T,k} + i\omega_{T,k})\widehat{T}_{k,t}\,dt - \alpha\hat{v}_{k,t}\,dt, \tag{20}$$

where

$$\gamma_{T,k} = d_T + \kappa k^2, \qquad \omega_{v,k}(t) = a_k u_t + b_k, \qquad \omega_{T,k}(t) = -u_t k. \tag{21}$$

The noise in eq. (19) is a complex Wiener process, $B_{k,t} = (B^1_{k,t} + iB^2_{k,t})/\sqrt{2}$, with $B^i_{k,t}$ being independent, real Wiener processes, such that $W_v(x,t) = \sum_k B_{k,t} e^{ikx}$. Also, in order for v_t to be real valued, we require $\hat{v}_{-k,t} = \hat{v}^*_{k,t}$, which is enforced through the constraints on:

$$\gamma_{v,k} = \gamma_{v,-k}, \quad a_k = -a_{-k}, \quad b_k = -b_{-k}, \quad B_{k,t} = B^*_{-k,t}, \tag{22}$$

and the real valued constraint for T_t is automatically satisfied.

2.2 Shear flow velocity field models

The stochastic zonal cross sweep dynamics in eq. (8) and the shear flow in eq. (11) can model a wide range of interesting turbulent flows. For the shear flow, several relevant models include random flows, non-dispersive waves, and quasi-geostrophic (QG) baroclinic 1.5 layer flows:

- Random flows:
$$\gamma_{v,k} = d_v + \nu k^2, \quad a_k = b_k = 0, \tag{23}$$
where ν is the flow viscosity.

- Non-dispersive waves:
$$\gamma_{v,k} = d_v + \nu k^2, \quad a_k = 0, \quad b_k = -ck, \tag{24}$$
with wave speed c. In this model, zonal flow is uncoupled from the shear flow since $a_k = 0$. This model is commonly encountered in the engineering community.

- β-plane quasi-geostrophic (QG) baroclinic 1.5 layer flows: This model [6, 16] has parameters
$$\gamma_{v,k} = d_v + \nu k^2, \quad a_k = \frac{-k^3}{k^2+F}, \quad b_k = \frac{\beta k}{k^2+F}, \tag{25}$$
where $F = L_R^{-2}$ and L_R is the deformation radius of Rossby waves, β represents rotation due to Coriolis forcing. This dispersive wave model has implications for atmosphere-ocean science modeling.

The prescribed energy spectrum $E_{v,k}$ for the shear flow sets the strength of the white noise forcing $\sigma_{v,k}$ for each wavenumber for v_k. In section 3, we show that the statistics of the shear flow is Gaussian, with energy spectra given by

$$E_{v,k} = \frac{\sigma^2_{v,k}}{2\gamma_{k,v}}, \tag{26}$$

so that the noise for the kth mode is set by $\sigma_k = \sqrt{2\gamma_{v,k}E_{v,k}}$. Example variance spectra for the shear flow include equipartition (white noise), Kolmogorov spectrum, and a combined spectrum with equipartition for the large scale modes and a Kolmogorov spectrum for the small scales:

- Equipartition spectrum (white noise)
$$E_{v,k} = E_0, \quad \text{for all } k. \tag{27}$$

- Kolmogorov spectrum
$$E_{v,k} = E_0|k|^{-5/3}. \tag{28}$$

- Combined spectrum:
$$E_{v,k} = \begin{cases} E_0, & |k| \le k_0, \\ E_0\left|\frac{k}{k_0}\right|^{-5/3}, & |k| > k_0, \end{cases} \tag{29}$$
which mimics realistic energy spectrum for large scale waves.

To investigate tracer intermittency in representative models, we analyze various shear flow configurations and their corresponding energy spectra.

2.3 Zonal flow velocity models

The zonal cross sweep velocity is decomposed into a constant mean $\overline{u}$ and a stochastic fluctuating term u'_t around the mean, $u_t = \overline{u} + u'_t$. Here we discuss various types of models for the zonal flow and their statistical properties. In section A.1 further details are provided.

2.3.1 Linear zonal model

The simplest stochastic zonal flow model is a forced Ornstein–Uhlenbeck (OU) type process given by

$$du_t = (-\gamma_u u + f)\, dt + \sigma_u\, dW_t, \tag{30}$$

with constant forcing f. The steady-state mean, variance and the invariant probability density function for such a linear model are easily obtained from the associated Fokker-Planck equation and are given by, respectively,

$$\overline{u} = \mathbb{E}(|u_\infty|) = \frac{f}{\gamma_u}, \quad E_u = \mathbb{E}(|u_\infty|^2) = \frac{\sigma_u^2}{2\gamma_u}, \quad p_u = \mathcal{N}(\overline{u}, E_u), \tag{31}$$

where $\mathcal{N}(\mu, \Gamma)$ denotes a real valued Gaussian with mean μ and variance Γ. It is possible to consider time dependent forcing leading to non-constant mean flows, however we refrain from this generalization. With constant forcing, the zonal flow fluctuations are simply offset by $\overline{u}$. A numerical simulation of a sample realization along with the equilibrium probability density function (PDF) is shown in fig. 1.

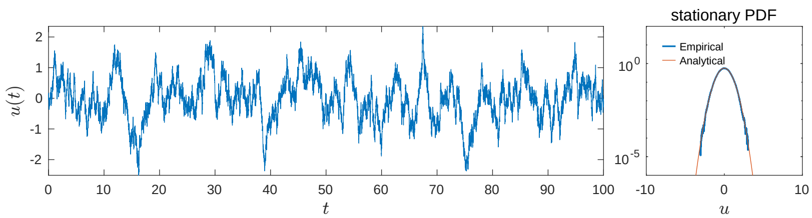

Figure 1 Sample realization and equilibrium PDF for the linear zonal model ($\gamma_u = 1, \sigma_u = 1$).

2.3.2 Non-linear zonal model

To capture the inherent non-Gaussianity and multiscale dynamics of geophysical flows, we extend our analysis to a more general class of stochastic models for zonal jet dynamics, characterized by cubic nonlinearity and correlated additive-multiplicative (CAM) noise structure:

$$du_t = (au_t + bu_t^2 - cu_t^3 + f)\, dt + (A - Bu_t)\, dW_2 + \sigma_u\, dW_1, \tag{32}$$

This system represents the simplest example of dynamics given by low-frequency reductions of large-scale climate dynamics and is the normal form for scalar stochastic climate models obtained via the stochastic mode reduction strategy [8]. We require $c > 0$ to ensure mean stability and is thus a cubic damping term, and W_1, W_2 are independent Wiener processes, where the term $(A - Bu_t)dW_2$ is referred to as correlated additive and multiplicative (CAM) noise.

For the special case with zero CAM noise, i.e. $A = B = 0$, eq. (32) is a standard gradient stochastic differential equation

$$dx_t = -\nabla V(x_t)\, dt + \sigma\, dW_t, \tag{33}$$

with potential $V(x_t)$ and the stationary distribution $p(x) = N_0 e^{-2V(x)/\sigma^2}$, where N_0 is a normalization constant. The explicit form of the potential for eq. (32) is given by

$$V_u(x) = -fx - \frac{a}{2}x^2 - \frac{b}{3}x^3 + \frac{c}{4}x^4. \tag{34}$$

The stationary probability measure for the general form with CAM noise, can be shown to be given by

$$p_u(u) = \frac{N_0}{((Bx - A)^2 + \sigma_u^2)^{a_1}} \exp\left(d \arctan\left(\frac{Bx - A}{\sigma_u}\right)\right) \exp\left(\frac{-c_1 x^2 + b_1 x}{B^4}\right), \tag{35}$$

where N_0 is a normalization constant. The coefficients a_1, b_1, c_1, d are provided in section A.2.

In remainder of the article we concentrate on models with $A = 0$:

$$du_t = (au_t + bu_t^2 - cu_t^3 + f)\, dt + Bu_t\, dW_2 + \sigma_u\, dW_1, \tag{36}$$

as it retains the main features interesting features that occur from multiplicative noise. This model with $b = c = 0$ and $a = -\gamma_u$ the model reduces to the OU process in section 2.3.1 when $B = 0$.

Numerical experiments. We present several test cases to demonstrate the dynamics of nonlinear zonal fluctuations across different parameter regimes. Throughout these experiments, the additive noise is maintained at a moderate value, $\sigma_u = 1$. We identify prototypical cases by fixing $c = 1$ and $b = 0$, as these parameters do not substantially alter the conclusions. Based on the stability analysis of the nonlinear cubic model in (a, f) parameter space (see section A.1), we investigate two distinct test cases.

In the first scenario, we set the multiplicative noise to zero ($B = 0$) as shown in fig. 2. The regime with $a = 2$ and $f = 0$ exhibits two metastable fixed points with stochastic switching. The transition frequency depends on the parameters and can be precisely controlled. In the second test case, we set the additive forcing to $f = -1.5$, placing the system outside the regime with two stable fixed points. Here, the system demonstrates non-Gaussian behavior with positive skewness, where the locally quadratic potential dominates the PDF, which remains approximately Gaussian for moderate values of σ_u.

In fig. 3, we examine the same test cases in (a, f) parameter space but set $B = 2.5$ to demonstrate the distinctive effects of multiplicative noise. The numerical experiments reveal that strong multiplicative noise induces significant skewness and inhibits the switching behavior characteristic of the double-well potential observed in the absence of multiplicative noise. This phenomenon occurs because the multiplicative noise accelerates fluctuations beyond the stable equilibria, where the system subsequently experiences strong damping, returning the signal toward zero. The system predominantly resides near zero, where the effect of multiplicative noise is minimal. This behavior produces stationary probability distributions characterized by unimodality and pronounced skewness, as evidenced in simulations.

3 Tracer model general properties and trajectory solution

The tracer model in eq. (18) has two fundamental properties. First, correlation between different Fourier modes occurs exclusively through the zonal flow u_t. Second, the dynamics of $\hat{v}_{k,t}$ and $\widehat{T}_{k,t}$ are linear and *conditionally Gaussian* given a fixed realization of u_t. This conditional Gaussianity can be exploited for efficient filtering and prediction (see [5, 2]), and is used here to analytically determine the solution of $\widehat{T}_{k,t}$, including its limiting stationary distribution.

A noteworthy characteristic of this system is that *it possesses no positive Lyapunov exponents, yet exhibits intermittent non-Gaussian solutions and extreme events*—a signature of systems containing intermittent instabilities. This property can be verified from eq. (18) by observing that the system is positively damped ($\lambda_{T,k}, \lambda_{v,k} > 0$), so checking Lyapunov stability is trivial. These properties will be demonstrated through numerical experiments presented in subsequent sections.

For simplicity, we can assume $\hat{v}_{k,0}$ and $\widehat{T}_{k,0}$ are initialized from zero. By integration, we have the shear flow trajectory solution

$$\hat{v}_{k,s} = \int_0^s \exp(-\gamma_{v,k}(s-r) + i\omega_{v,k}[r,s])\sigma_{v,k}\, dB_{k,r}. \tag{37}$$

The expression $X[r,s]$ is used to denote the integral $X[r,s] := \int_r^s X_u du$, thus $\omega_{v,k}[r,s]$ represents the accumulated phase. We see that $\hat{v}_{k,s}$ is a complex Gaussian with mean and variance, respectively,

$$\mathbb{E}(\hat{v}_{k,s}) = 0, \qquad \mathbb{E}(|\hat{v}_{k,s}|^2) = E_{v_k}(1 - e^{-2\gamma_{v,k}s}), \quad \text{where } E_{v_k} = \frac{\sigma_{v,k}^2}{2\gamma_{k,v}}. \tag{38}$$

In the long time limit $s \to \infty$, the shear flow converges to a Gaussian probability measure $\pi_{\hat{v}_k} = \mathcal{CN}(0, E_{v_k})$, where $\mathcal{CN}(\mu, \Gamma)$ denotes a complex Gaussian with mean μ and variance Γ.

Similarly, we can integrate the equation for $\widehat{T}_{k,t}$ using the result eq. (37).

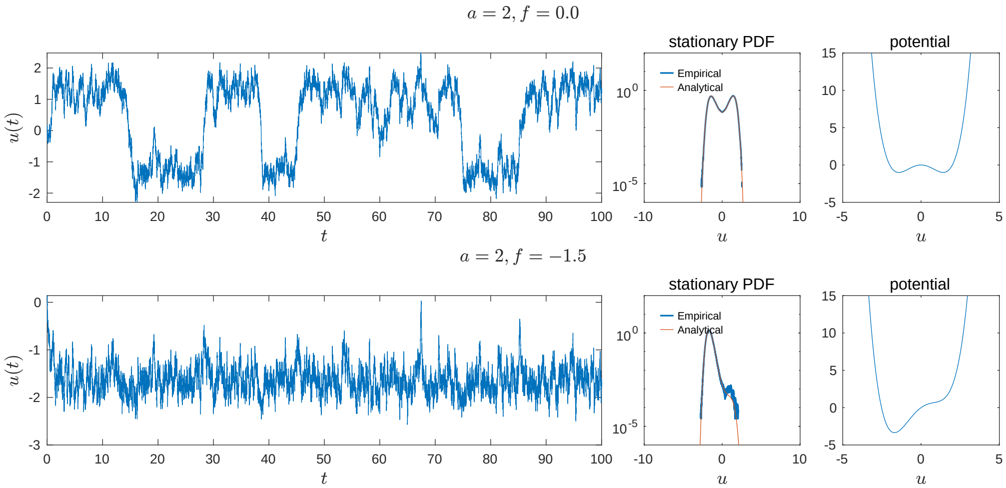

Figure 2 Sample realization, equilibrium PDF, and potential for the nonlinear zonal model without multiplicative noise, $B = 0$.

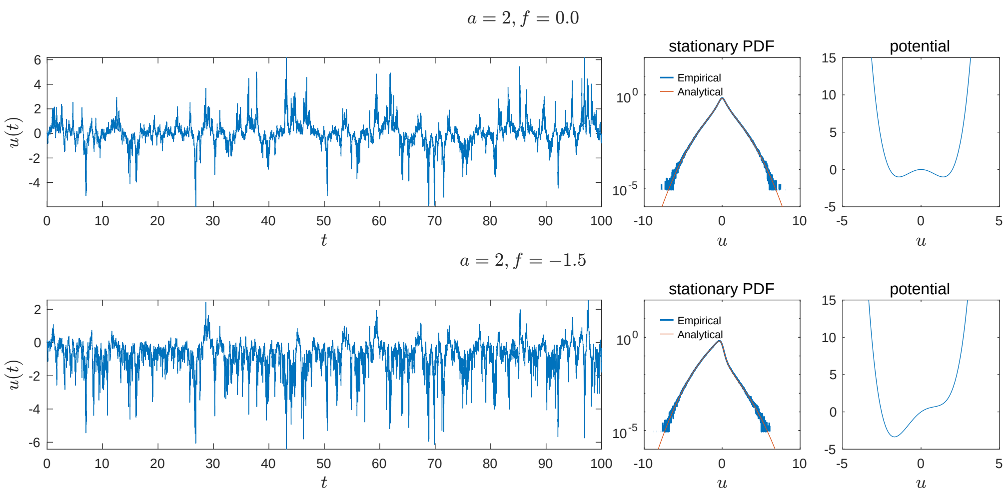

Figure 3 Sample realization, equilibrium PDF, and potential for the nonlinear zonal model with multiplicative noise, $B = 2.5$.

Proposition 3.1. *The exact trajectory solution of the tracer model is given by*

$$\widehat{T}_{k,t} = \int_0^t -\alpha \exp(-\gamma_{T,k}(t-s) + i\omega_{T,k}[s,t])\hat{v}_{k,s}\, ds \tag{39}$$

$$= \int_0^t \int_r^t -\alpha\sigma_{v,k} \exp(-\gamma_{T,k}(t-s) - \gamma_{v,k}(s-r) + +i\omega_{T,k}[s,t] + i\omega_{v,k}[r,s])\, ds\, dB_{k,r}. \tag{40}$$

From the trajectory solution, conditioned on a zonal flow trajectory u_t, we find that $\widehat{T}_{k,t}$ is a complex Gaussian random variable $\mathcal{CN}(0, \Sigma_{k,t|u})$, with zero mean and variance given by the following result.

Proposition 3.2. *The conditional variance of a trajectory solution is given by*

$$\Sigma_{k,t|u} = \alpha^2\sigma_{v,k}^2 \int_0^t \left| \int_r^t \exp(-\gamma_{T,k}(t-s) - \gamma_{v,k}(s-r) + +i\omega_{T,k}[s,t] + i\omega_{v,k}[r,s])\, ds \right|^2 dr \tag{41}$$

$$= \alpha^2\sigma_{v,k}^2 \int_0^t \exp(-2\gamma_{v,k}(t-r)) \left| \int_r^t \exp(-\gamma_{R,k}(t-s) + i\omega_{R,k}[s,t])\, ds \right|^2 dr, \tag{42}$$

where $\gamma_{R,k} \coloneqq \gamma_{T,k} - \gamma_{v,k}$ and

$$\omega_{R,k} \coloneqq \omega_{T,k} - \omega_{v,k} = -(a_k + k)u_t - b_k.$$

x Alternatively, we can express the variance as:

$$\Sigma_{k,t|u} = \alpha^2 \sigma_{v,k}^2 \int_0^t \exp(-2\gamma_{v,k}(t-r)) \left| \int_r^t \exp(-\gamma_{R,k}(t-s) + i\omega_{R,k}[s,t]) \, ds \right|^2 dr. \tag{43}$$

Corollary 3.3. *An upper bound on the conditional variance is given by*

$$\Sigma_{k,t|u} \leq \frac{\alpha^2 \sigma_{v,k}^2}{\gamma_{R,k}^2} \left(\frac{1}{2\gamma_{v,k}} + \frac{1}{2\gamma_{T,k}} \right) \tag{44}$$

4 Tracer model statistical solutions

In this section, we focus on the case where the velocity field $(u_t, v_t(x))$ evolves slowly compared to the advection and diffusion processes. This assumption is a natural condition for the dynamics of atmosphere-ocean systems, where large-scale flows typically vary on slower timescales compared to the small-scale turbulent motions they influence. To incorporate this separation of scales, we scale the governing equations in Fourier space for the zonal and shear flow dynamics by a small parameter ϵ.

Under this formulation, the Fourier space model for the cross sweeps and shear flow are scaled by ϵ, so that eq. (18) takes the form

$$du_t = \epsilon f(u_t) \, dt + \sqrt{\epsilon} \sigma(u_t) \, dW_t, \tag{45}$$

$$d\hat{v}_{k,t} = (-\epsilon \gamma_{v,k} + i\omega_{v,k}) \hat{v}_{k,t} \, dt + \sqrt{\epsilon} \sigma_{v,k} \, dB_{k,t}, \tag{46}$$

$$d\widehat{T}_{k,t} = (-\gamma_{T,k} + i\omega_{T,k}) \widehat{T}_{k,t} \, dt - \alpha \hat{v}_{k,t} \, dt. \tag{47}$$

The frequency $\omega_{v,k}$ is not scaled by ϵ, since it represents the internal wavelike effects of the cross sweeps on v_t (which should be on the same scale), and the equation for $\widehat{T}_{k,t}$ is exactly as before, but here the advection term due to the shear flow is slowly varying.

To study the dynamics on a long timescale, we consider the rescaled time $t' = \epsilon t$. Substituting this into the governing equations (and dropping primes for clarity) gives the following

Definition 4.1. *On long timescales the turbulent shear model under slowly varying velocity fields is given by*

$$du_t = f(u_t) \, dt + \sigma(u_t) \, dW_t, \tag{48}$$

$$d\hat{v}_{k,t} = (-\gamma_{v,k} + i\epsilon^{-1} \omega_{v,k}) \hat{v}_{k,t} \, dt + \sigma_{v,k} \, dB_{k,t}, \tag{49}$$

$$d\widehat{T}_{k,t} = \epsilon^{-1} (-\gamma_{T,k} + i\omega_{T,k}) \widehat{T}_{k,t} \, dt - \epsilon^{-1} \alpha \hat{v}_{k,t} \, dt, \tag{50}$$

where the time dependent frequencies are given by

$$\omega_{v,k} = a_k u_t + b_k, \quad \omega_{T,k} = -u_t k. \tag{51}$$

This rescaled system reveals a separation of timescales. As ϵ approaches zero, the velocity field (u_t, v_t) evolves much more slowly than the tracer field. This separation allows us to treat the velocity field as approximately constant when analyzing the rapid fluctuations in the tracer dynamics, while capturing the long-term evolution of the flow structure.

4.1 Limiting distribution for tracer statistics

An approximate analytical result for the stationary distribution for the tracer statistics can be derived by analyzing the steady-state conditional variance $\Sigma_{k,t|u}$. Since the tracer trajectory is a conditional Gaussian integral, given u_t, its full distribution can be expressed using the law of total probability. The stationary distribution of the real part of the tracer mode $\mathrm{Re}(\widehat{T}_k)$ is then

$$p(x) = \int \frac{1}{\sqrt{\pi \widetilde{\Sigma}_k(u)}} \exp\left(-\frac{x^2}{\widetilde{\Sigma}_k(u)} \right) p_u(u) \, du. \tag{52}$$

Where, $\widetilde{\Sigma}_k(u)$ is the stationary value of the conditional variance $\Sigma_{k,t|u}$.

Proposition 4.2. *Under slowly varying velocity fields, the conditional tracer variance converges to the stationary value*

$$\widetilde{\Sigma}_k(u) = \frac{\alpha^2 E_{v,k}}{\gamma_{T,k}^2 + \omega_{R,k}(u)^2}. \tag{53}$$

In the stationary limit, u is treated as a static parameter sampled from its steady state distribution.

The steady-state distribution of the passive scalar is obtained by the same approach, additionally summing over all wavenumbers.

Theorem 4.3. *The stationary distribution of the tracer field $T(x)$ for the model in eq. (48) is given by:*

$$p(\lambda) = \int \frac{1}{\sqrt{2\pi\widetilde{\Sigma}(u)}} \exp\left(-\frac{\lambda^2}{2\widetilde{\Sigma}(u)}\right) p_u(u)\, du, \tag{54}$$

where

$$\widetilde{\Sigma}(u) = \sum_{k\in\mathbb{N}} \frac{\alpha^2 E_{v,k}}{\gamma_{T,k}^2 + \omega_{R,k}(u)^2} \tag{55}$$

4.2 Intermittency and extreme events through resonance

Extreme events in the turbulent tracer field are linked to peaks in the conditional variance. Inspecting eq. (55) we see that the conditional variance reaches its maximum when $\omega_{R,k} \coloneqq \omega_{T,k} - \omega_{v,k} = 0$, which corresponds to a resonant condition when the phase speeds of the zonal flow, shear flow, and tracer field align, i.e. $\omega_{T,k} = \omega_{v,k}$ This resonance leads to bursts in the tracer field variance, occurring when $\omega_{R,k} = 0$ or

$$u_t' + \overline{u} = u_{\text{res},k} \coloneqq -\frac{b_k}{a_k + k} \tag{56}$$

$$u_t' = u_{\text{res},k}' \coloneqq -\frac{b_k}{a_k + k} - \overline{u} \tag{57}$$

which define the resonant phase speeds. *When the zonal flow fluctuations u_t' crosses the phase speed threshold $u_{res,k}'$ the wavenumbers $\pm k$ are excited, producing an intermittent burst.* Unlike intermittency in unstable systems—where finite-time instabilities yield heavy-tailed statistics and bursts—this mechanism is resonance-driven: fluctuations in the zonal flow trigger resonance, amplifying the conditional variance and causing non-Gaussian tracer statistics.

For deterministic periodic shears this 'resonance' driven intermittency was first noted in [1] and was linked to a physical interpretation of 'blocked' and 'un-blocked' streamlines. In this interpretation when the zonal flow is $u \approx 0$ the shear flow is unblocked leading to strong convective transport of the tracer along the direction parallel to the mean scalar gradient and strong mixing by diffusion. Conversely, when $u \neq 0$, the transverse sweeps are blocked and transport along the gradient is minimal. The resonance condition eq. (56) can be interpreted as a generalization of this result to stochastic zonal and shear flows.

Understanding how the zonal and shear flows affect tracer statistics is crucial, especially the role of nonlinearity in the zonal flow. While zonal fluctuations do not change the resonant phase speeds—these are set by the wave dynamics of the shear flow and zonal mean—they do influence how often the system crosses resonance, thus modulating tracer statistics (see eq. (54)). This means that the statistics of the nonlinear zonal flow can act to either enhance turbulent tracer transport through increased intermittency or reduce intermittency relative to a linear (Gaussian) flow model. This underscores the importance of the zonal flow's stochasticity in the tracer field intermittency, and has implications for linearization approaches.

Although the shear flow does not directly affect the frequency that resonance is reached—the zonal flow statistics determine this—wavelike effects in the shear modify the resonant phase speed values. This influences how often the zonal flow crosses these thresholds. In a purely random shear flow with no wavelike effects, where $a_k = b_k = 0$ (see eq. (23)), the resonant speeds collapse to a single value:

$$u_{\text{res}}' = -\overline{u}; \tag{58}$$

A similar synchronization appears in non-dispersive advection, where $a_k = 0$ and $b_k = -ck$:

$$u'_{\text{res}} = c - \overline{u}. \tag{59}$$

In both cases, crossing the resonance threshold excites all modes simultaneously, leading to stronger intermittency, as every excited mode contributes to the tracer field. This also produces finer-scale structures during extreme events due to the excitation of higher-wavenumber modes.

In contrast, dispersive shear flows yield multiple resonant phase speed thresholds (one for each wavenumber k), whereas purely random shear flows and non-dispersive advection synchronize these thresholds, exciting all scales at once. This distinction strongly influences the nature of intermittency and the structure of extreme tracer events.

5 Numerical experiments and regimes for a single mode

We now perform numerical experiments to examine the effect of zonal and shear flows on tracer intermittency and extreme events across various regimes.

We first consider a single tracer mode, i.e. $k = 1$, and assume the shear flow is described by the β-plane QG model in eq. (25). Unless stated otherwise, we consider a system with the following parameters

$$\epsilon = 0.010, \quad d_T = 0.1, \quad \kappa = 0.001, \quad d_v = 0.6, \quad \nu = 0.1, \quad \alpha = 1, \quad \beta = 8.91, \quad F = 16. \tag{60}$$

5.1 Numerical integration

Integration of the multiscale tracer model in eq. (48) requires some special care. The zonal flow u_t is integrated using an explicit Euler-Mayurama scheme, while $\hat{v}_{k,t}$ and $\widehat{T}_{k,t}$ are updated using an exact exponential-integrator scheme. The updates for step Δ are given as follows:

$$u_{t+\Delta} = u_t + f_U(u_t)\Delta + \sigma_U(U)\Delta w_t \tag{61}$$

$$\hat{v}_{k,t+\Delta} = \exp\big((-\gamma_{v,k} + i\epsilon^{-1}\omega_{v,k}(t))\Delta\big)\hat{v}_{k,t} + \sigma_{v,k}\sqrt{\Delta \exp\big((-\gamma_{v,k} + i\epsilon^{-1}\omega_{v,k}(t))\Delta\big)}\,\frac{b_t^1 + ib_t^2}{\sqrt{2}} \tag{62}$$

$$\widehat{T}_{k,t+\Delta} = \exp\big(\epsilon^{-1}(-\gamma_{T,k} + i\omega_{T,k})\Delta\big)\widehat{T}_{k,t} - \epsilon^{-1}\alpha\Delta \exp\big(\epsilon^{-1}(-\gamma_{T,k} + i\omega_{T,k})\Delta\big)\hat{v}_{k,t} \tag{63}$$

where

$$\gamma_{T,k} = d_T + \kappa k^2, \quad \omega_{v,k} = a_k u_t + b_k, \quad \omega_{T,k} = -ku_t, \tag{64}$$

and w_t, b_t^1,b_t^2 are independent uniform Gaussian random variables.

5.2 Stochastic zonal mean flow with linear dynamics

Consider a zonal flow described by the OU process in eq. (30). with statistics in eq. (31). We consider a case where the eastward zonal jet has the following parameters: $E_u = 0.5$ (with $\gamma_u = 1$ and $\sigma_u = 1$). The forcing is set to $f = 0.4431$, such that $u'_{\text{res}} = -1$, and so fluctuations crossing this threshold occur with probability $p(u < u'_{\text{res}}) = 0.0228$. At resonance (when $u = u'_{\text{res}}$), the conditional Gaussian variance increases dramatically, with $\Sigma(u'_{\text{res}}) > 87\Sigma(\overline{u})$, indicating an 87-fold amplification compared to the mean flow condition.

In fig. 4 we plot the limiting equilibrium PDF along with the histogram of the time series and the corresponding realizations of the tracer mode for various ϵ. At any fixed time, the tracer distribution is Gaussian, however the variance is time dependent and shoots at zero crossings of the frequency ω_R or equivalently when the zonal flow fluctuations u'_t crosses u'_{res}. Furthermore, as $\epsilon \to 0$ intermittency is enhanced since the slowly varying zonal flow u_t spends a longer period of time in the resonance regime leading to larger extreme events. We note the close agreement between the analytical result and the histogram of the time series as ϵ tends to zero.

5.3 Stochastic zonal mean flow with nonlinear dynamics

We now consider the nonlinear model in eq. (32). Motivated by the discussion and the regimes presented in section 2.3.2 we consider several representative cases with interesting statistics for the zonal flow, including cases with zero multiplicative noise $B = 0$ in fig. 5 and strong multiplicative noise $B = 2.5$ in fig. 6, with zonal flows that correspond to those in figs. 2 and 3. As in section 2.3.2, we set $\sigma_u = 1$ and set $c = 1$ and $b = 0$ throughout the analysis.

Some important points that these cases demonstrate in the single Fourier mode case is that *strong nonlinearity and non-trivial Gaussian statistics in the zonal flow, such as bimodal distributions or heavily skewed fat-tailed statistics, do not necessarily lead to enhanced tracer intermittency.* In fact, it is possible to observe a zonal flow with strongly non-Gaussian features compared to a linear case with Gaussian statistics, yet the tracer field PDF is nearly identical. This can be understood by the fact that the zero *crossing frequency of the resonance threshold* $\omega_R = 0$ *is of vital importance and this frequency is not uniquely determined by the form of the zonal flow dynamics*. Thus different zonal flows can lead to similar tracer statistics if their resonance crossing frequency are equivalent. This is a feature of the single mode case. Other interesting observations include the 'on-off' type intermittency regime in the double well zonal flow test case (case b, $B = 0$), and intermittency from 'below' in case c. As an aside, note that the analytical limiting tracer formula for the experiments with strong multiplicative noise do not agree as well to the cases with $B = 0$. This is expected since large multiplicative noise leads to a diffusion process that has a shorter time scale and thus the time scale separation between the zonal flow and tracer modes is decreased.

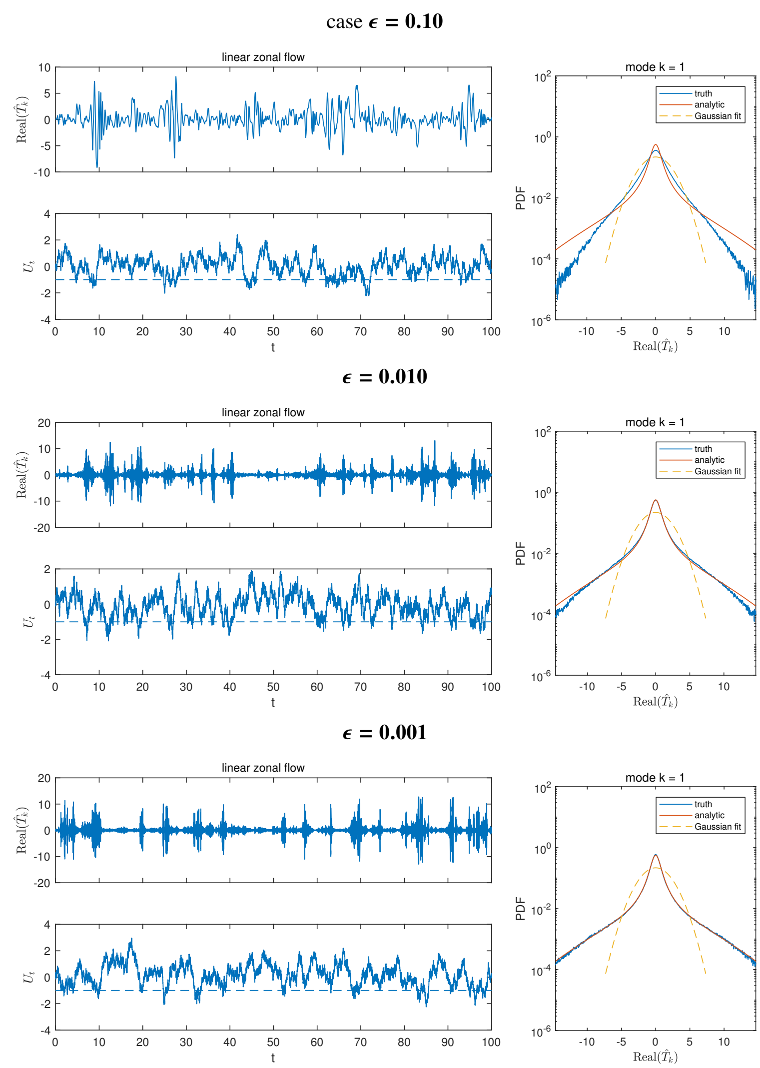

Figure 4 Sample realizations and the corresponding equilibrium pdfs and their analytical limit. Model: single mode, $k = 1$, β-plane QG flow. Linear zonal fluctuations with $E_u = 0.5$ ($\gamma_u = 1, \sigma_u = 1$). Dashed line in U_t plot is the resonance threshold $\omega_1^* = -1.0$.

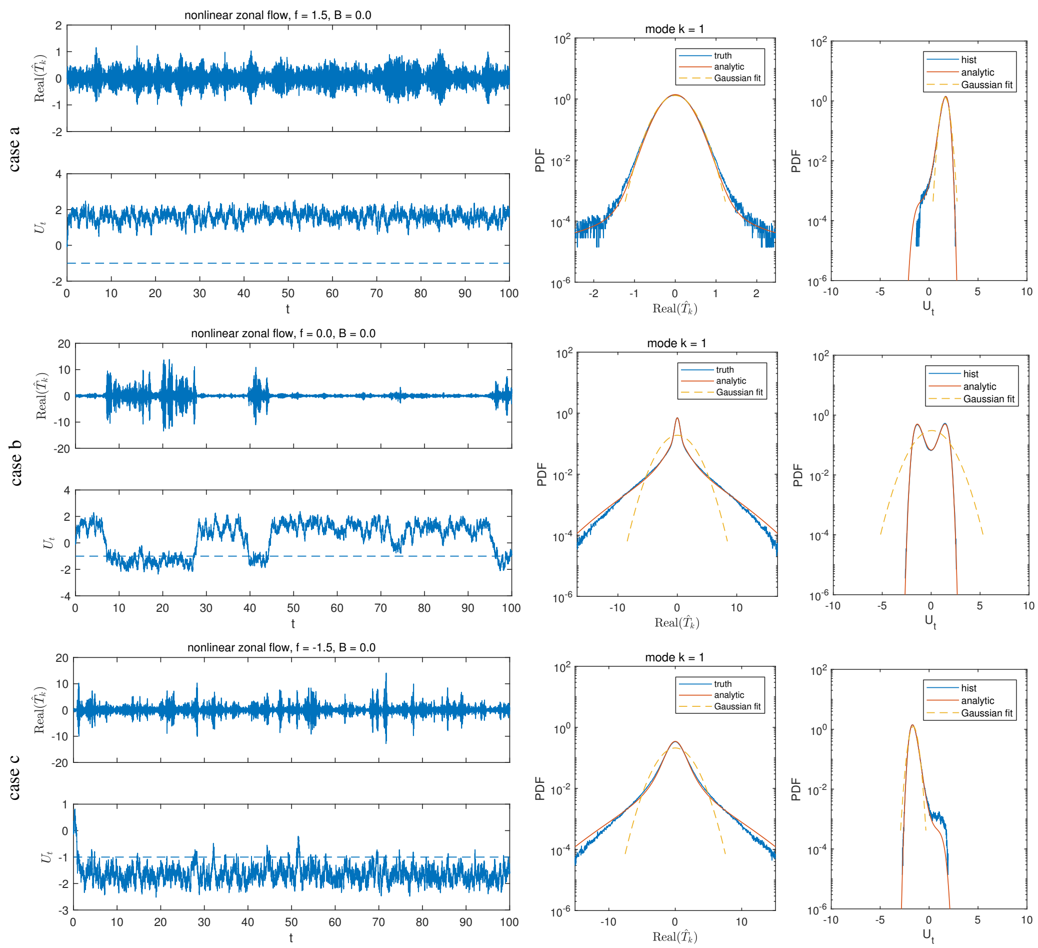

Figure 5 Sample realizations and the corresponding equilibrium pdfs and their analytical limit. Model: single mode, $k = 1$, β-plane QG flow. Nonlinear zonal fluctuations in various regimes with zero multiplicative noise. Dashed line in U_t plot is the resonance threshold $\omega_1^* = -1.0$.

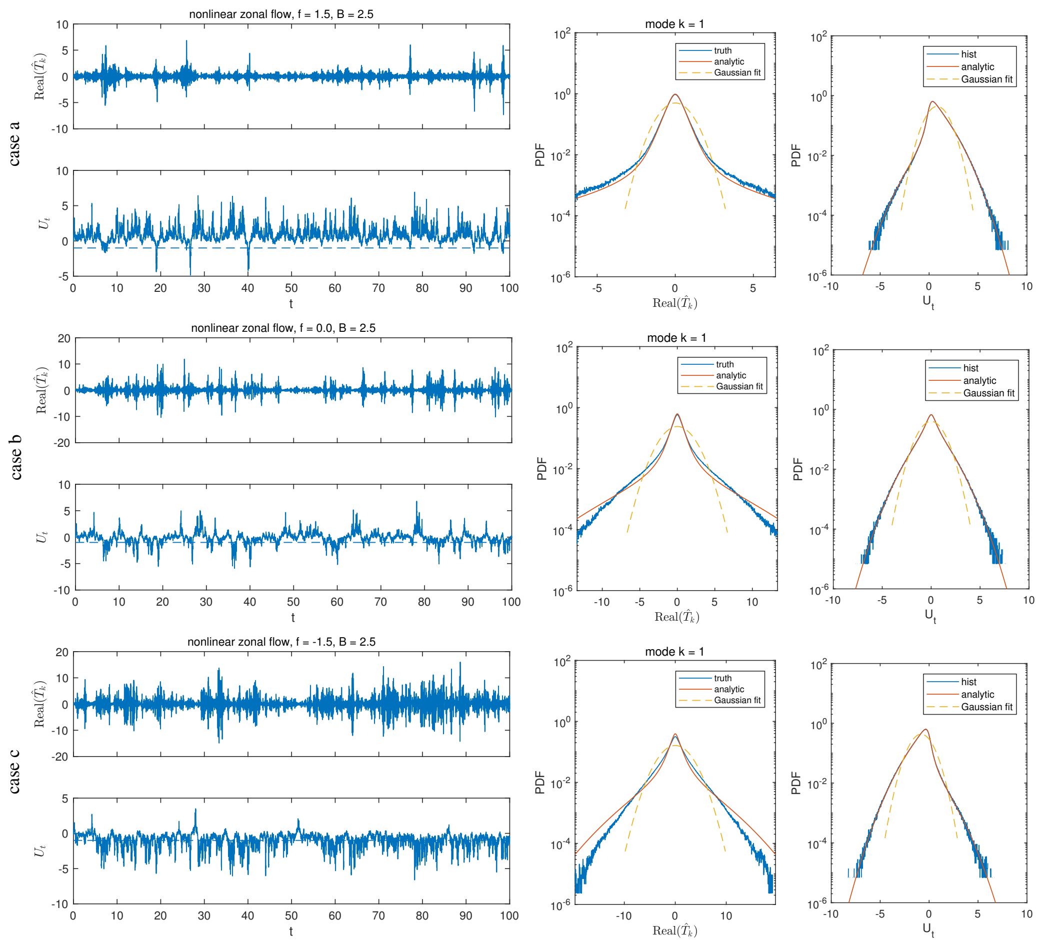

Figure 6 Sample realizations and the corresponding equilibrium pdfs and their analytical limit. Model: single mode, $k = 1$, β-plane QG flow. Nonlinear zonal fluctuations in various regimes with multiplicative noise $B = 2.5$. Dashed line in U_t plot is the resonance threshold $\omega_1^* = -1.0$.

6 Numerical experiments and regimes for finitely many Fourier mode

We now consider finitely many tracer modes and their effect on the distribution of the tracer field. Recall $T_t(x) = \sum_k \widehat{T}_{k,t} e^{ikx}$, with $\widehat{T}_{k,t} = \widehat{T}^*_{-k,t}$, which means that a finite number of modes have a combined effect on the tracer field statistics and intermittency. This is more clearly understood by looking at the formula for the conditional variance of the tracer field, which is simply the sum of the conditional variance for each mode (55):

$$\widetilde{\Sigma}(u) = \sum_{k\in N} \widetilde{\Sigma}_k(u) = \sum_{k\in N} \frac{\alpha^2 E_{v,k}}{\gamma_{T,k}^2 + (c_k u + d_k)^2}. \tag{65}$$

In the finitely many Fourier mode scenario we have more rich dynamics compared to the single Fourier mode situation, since the total variance is a sum of the conditional variance for each mode, which can have their variance peak at different zonal phase speeds. The fact that different modes may have different resonance levels, has an impact on the overall nature of extreme events in the tracer field. These points will be demonstrated in numerical experiments.

The energy spectrum of the shear flow $v_t(x)$ is set to either equipartition (27) or a Kolmogorov spectrum (28)[1]:

$$E_{k,v} = 1 \quad \text{(equipartition)} \qquad E_{k,v} = E_0|k|^{-5/3} \quad \text{(Kolmogorov)}. \tag{66}$$

We consider these two cases to demonstrate the effects of the energy level of the shear flow on extreme events. Under equipartition, each mode $\hat{v}_k$ has the same energy and thus during resonance crossings ω_k^* all excited modes will force the tracer mode with the same intensity $\hat{T}_k$ and induce a burst of roughly the same magnitude in all the excited modes (roughly, since the smaller scale modes are selectively damped, which means these modes contribute less to the magnitude of the extreme events). Contrast this to the Kolmogorov spectrum, where smaller scales in the shear flow have less energy and thus their excitation adds a smaller contribution to the total tracer field statistics. The tracer extreme event statistics will thus be essentially determined by the largest most energetic scales.

6.1 Numerical experiments

As in the single Fourier case, we consider the β-plane QG flow model eq. (25) as a representative wavelike, dispersive shear flow, with the following parameters

$$\overline{u} = 0.4171, \quad d_T = 0.1, \quad \kappa = 0.001, \quad d_v = 0.6, \quad \nu = 0.1, \quad \alpha = 1, \quad \beta = 8.91, \quad F = 16. \tag{67}$$

We include results for $\epsilon = 0.01$ and for the set of wavenumbers $k \in \{-5, \dots, 5\}$, unless otherwise stated.

6.1.1 Stochastic zonal mean flow with linear dynamics

In fig. 7 we compare the results under linear zonal fluctuations with an equipartition spectrum and Kolmogorov spectrum. Observe the multiple resonance thresholds ω_k^*, which are plotted in dashed lines in the figure showing the zonal flow trajectory U_t. All the bursts in the time sequence of the tracer modes and the tracer field can be predicted from the resonance crossings of U_t. The high frequency modes, i.e. large k, have thresholds that are far from the mean of U_t and are increasingly rare to cross and, consequently, the contribution to the overall tracer statistics is smaller. *Under equipartition, we have more extreme and intermittent tracer statistics and prominent smaller scale spatial features in the tracer field compared to a Kolmogorov spectrum.* This can easily be understood by the fact that when we have multiple resonance threshold crossings, all the excited modes have the same energy level and consequently all the modes contribute significantly to the tracer field statistics. This can also be observed in the conditional variance $\widetilde{\Sigma}$ for equipartition, where we see multiple peaks corresponding to the resonance thresholds and that the peaks corresponding to the high frequency modes have large magnitude, comparable to the lowest frequency modes. This is in contrast to the Kolmogorov spectrum, where the high frequency modes have less energy and contribute minimally to the overall tracer field statistics. Looking at the conditional covariance of the tracer field, we see that the contribution to the conditional variance of the resonance values ω_k^* of the higher frequency modes is overwhelmed by the variance of the first mode. This leads us to the following important point: *The largest energetic scales determine the statistics of the tracer field. Model reduction retaining the effects of these modes is an effective strategy.*

[1] We normalize the energy of the first mode $k = 1$ such that $E_{1,v} = 1$ for the Kolmogorov spectrum.

6.1.2 *Stochastic zonal mean flow with nonlinear dynamics*

We now investigate cases with the nonlinear zonal fluctuation formulation in section 2.3.2. As in the single Fourier mode case, we consider zonal flows corresponding to the regimes presented in section 2.3.2, including cases with zero multiplicative noise $B = 0$, fig. 8, and strong multiplicative noise $B = 2.5$, fig. 9, and as before we fix $\sigma_u = 1$ and consider cases with $c = 1$ and $b = 0$.

In section 5.3 we observed that nonlinearity and non-Gaussian zonal flow statistics in the single Fourier mode case can significantly effect tracer intermittency and extreme events. This is also true with multiple Fourier modes, but with additional features due to the non-synchronized resonance thresholds in dispersive flows. In particular, compared to linear zonal flows, we can have either enhanced or suppressed intermittency depending on the skewness and kurtosis of the zonal fluctuations, see fig. 9 which demonstrate cases with prominent skewness and kurtosis under multiplicative noise. Large kurtosis values imply an increase in the frequency of visiting the resonance thresholds of the smaller scale modes and thus lead to enhanced intermittency. Skewness of the zonal flow statistics, due to non-zero forcing, also greatly impact tracer intermittency, which can again be understood in terms of the frequency of visiting the resonance thresholds. When the forcing induces skewness towards the resonance values ('resonant' forcing), tracer intermittency is enhanced. Conversely, for a zonal flow with small Kurtosis values and skewness away from the the resonance thresholds ('non-resonant' forcing) we observe suppressed tracer intermittency and extreme events. The impact of these effects are of course enhanced in the equipartition range.

In fig. 8 we demonstrate time histories and tracer statistics for cases with zero multiplicative noise. Similar to the single Fourier mode case, we note in certain regimes, modes can actually be excited from 'below', in the sense that the zonal flow first excites the smallest tracer modes before the largest scales; See case b, with a double well potential, and case c, for examples of this phenomenon. This is in contrast to the usual case, where the largest scales are excited before smaller scales. Also note the distinct 'on-off' switching behavior of intermittency in these regimes, which coincides with the zonal flow transitioning between the two potential wells. The transition to the well with a fixed point below ω_1^*, induces this interesting 'on-off' intermittency regime.

In the single Fourier mode case we also noted that it was possible to observe very similar tracer field statistics under nonlinear conditions if the resonance crossing frequency of the zonal flow is equivalent to a case with linear stochastic dynamics. With finitely many Fourier modes in dispersive shear flows, where the resonance phase speeds are not all synchronized this is not necessarily possible since nonlinearity in the zonal fluctuations will impact the excitation frequency of all the modes, and since they are not synchronized, this will consequently lead to differences compared to linear conditions. This effect is of course more important under equipartition. In non-dispersive or random flows, it is possible to observe similar statistics if the resonance frequency is equivalent to linear conditions.

In summary, with finitely many Fourier modes, we have markedly different tracer statistics and new regimes compared to linear stochastic zonal flow regimes.

7 Comparative analysis of tracer intermittency and spatial structures in random and advective, wavelike shear flows

We now include a detailed comparison of tracer intermittency and tracer spatial features between different shear flow models and zonal flow conditions. Consider again the nonlinear zonal flow model in eq. (32):

$$dU_t = (aU_t + bU_t^2 - cU_t^3 + f)\,dt + BU_t dW_2 + \sigma_u dW_1. \tag{68}$$

Motivated by the discussion and the regimes presented in section 2.3.2 we consider several representative zonal flow regimes with interesting statistics, including **linear dynamics** (i.e. OU process, see fig. 1), **nonlinear dynamics** with strong **multiplicative noise** (fig. 3), and **double well potential** flow (fig. 2). In addition, we include cases, for the nonlinear flow where there is resonant forcing (in the sense that the non-zero forcing induces skewness in the flow that is favorable towards exciting resonance in the tracer modes) and non-resonant forcing. In table 1 the parameters for the test cases are provided. The remaining fixed system parameters are

$$\overline{u} = 1, \quad d_T = 0.1, \quad \kappa = 0.001, \quad d_v = 0.6, \quad \nu = 0.1, \quad \alpha = 1, \quad \epsilon = 0.01. \tag{69}$$

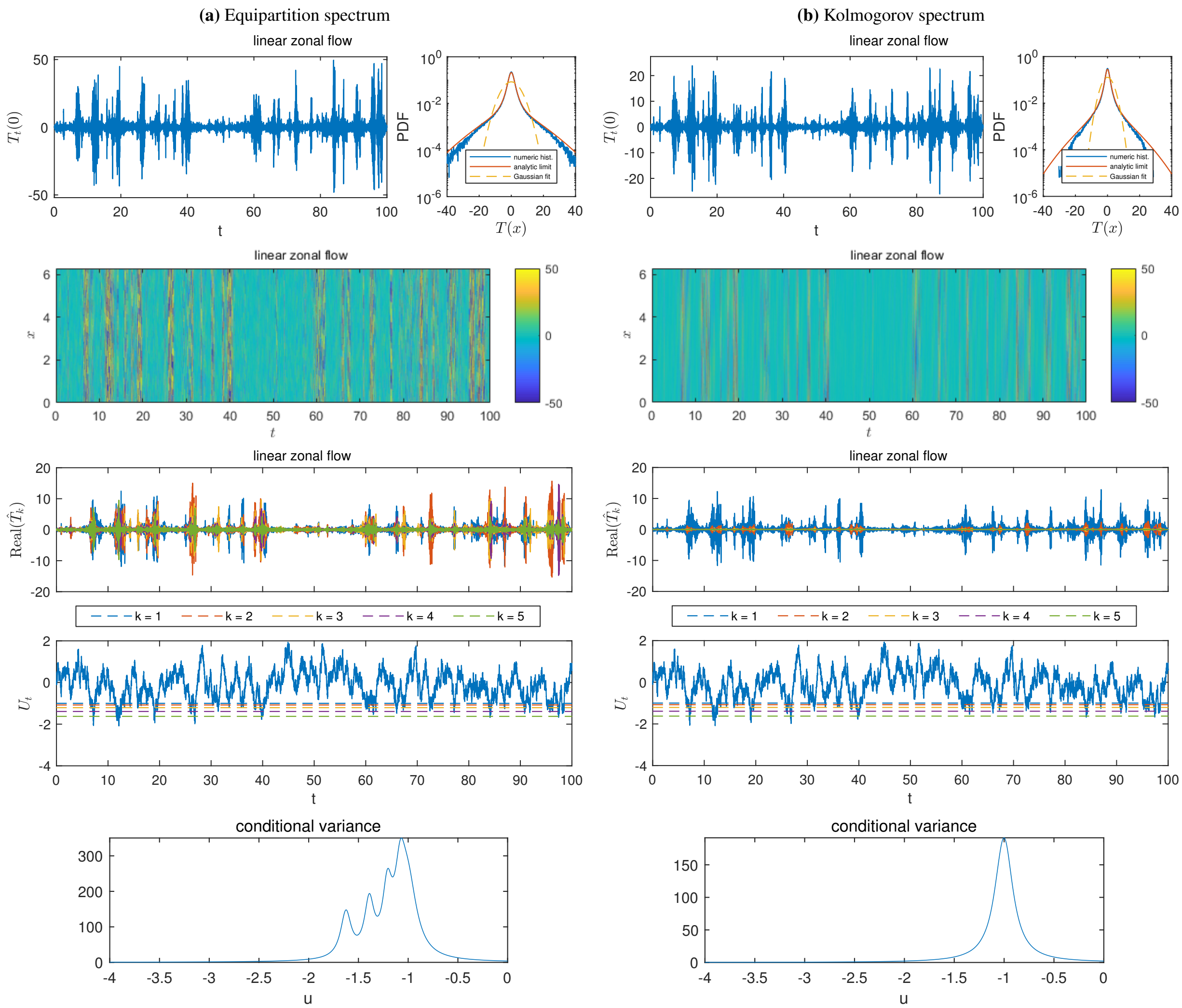

Figure 7 Multiple mode, β-plane QG flow. Linear zonal fluctuations with $E_u = 0.5$ ($\gamma_u = 1, \sigma_u = 1$).

Table 1 Zonal flow parameters for the test cases.

	f	a	b	c	σ_U	B
case l1 (linear)	0	-1	0	0	1	0
case n1 (nonlinear, double well)	0	2	0	1	1	0
case n2 (nonlinear, multiplicative noise)	0	2	0	1	1	2.5
case n3 (nonlinear, multiplicative noise, neg. skewness)	-1.5	2	0	1	1	2.5
case n4 (nonlinear, multiplicative noise, pos. skewness)	1.5	2	0	1	1	2.5

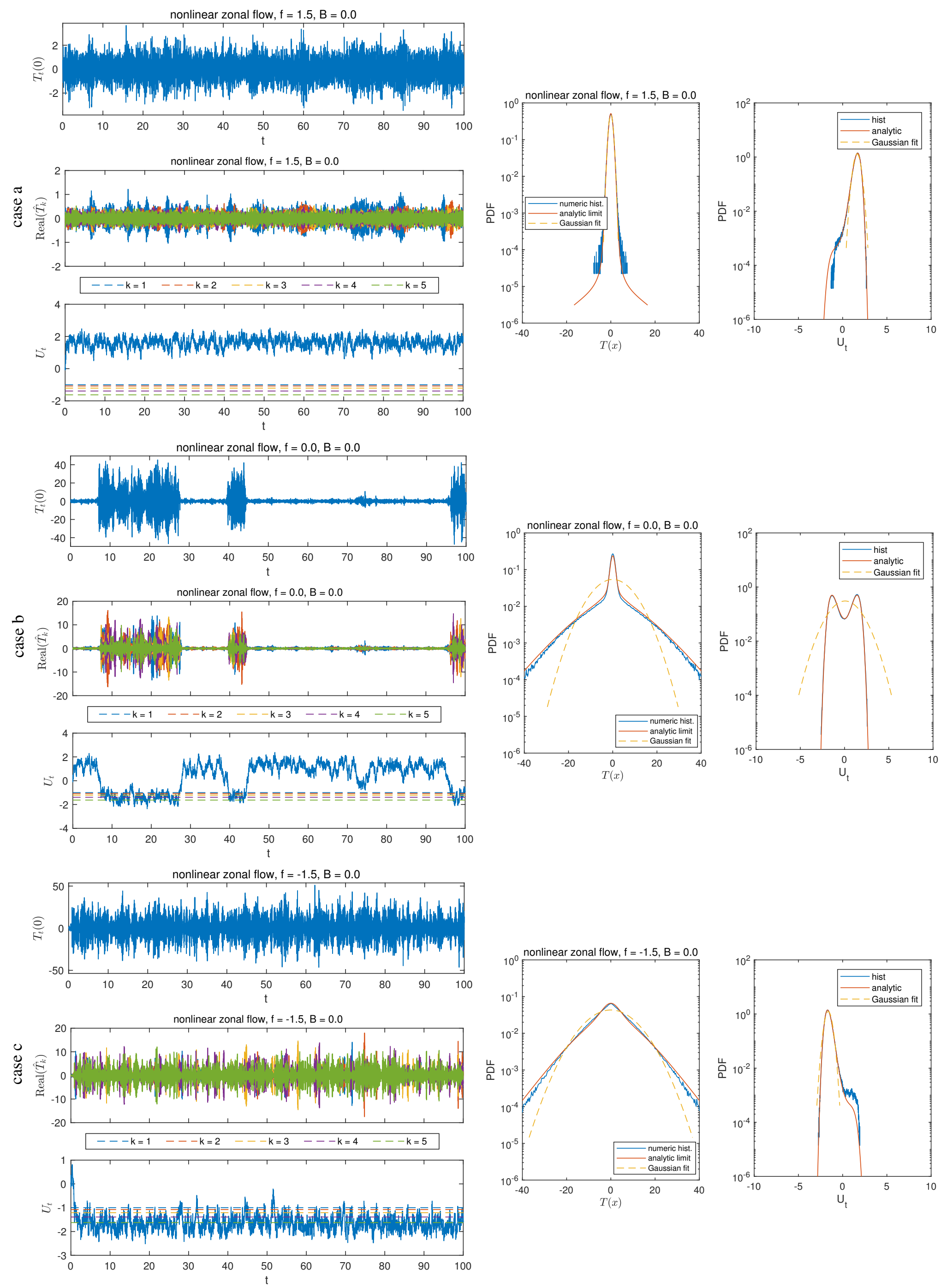

Figure 8 Multiple mode, β-plane QG flow. Nonlinear zonal fluctuations with zero multiplicative noise and equipartition shear spectrum.

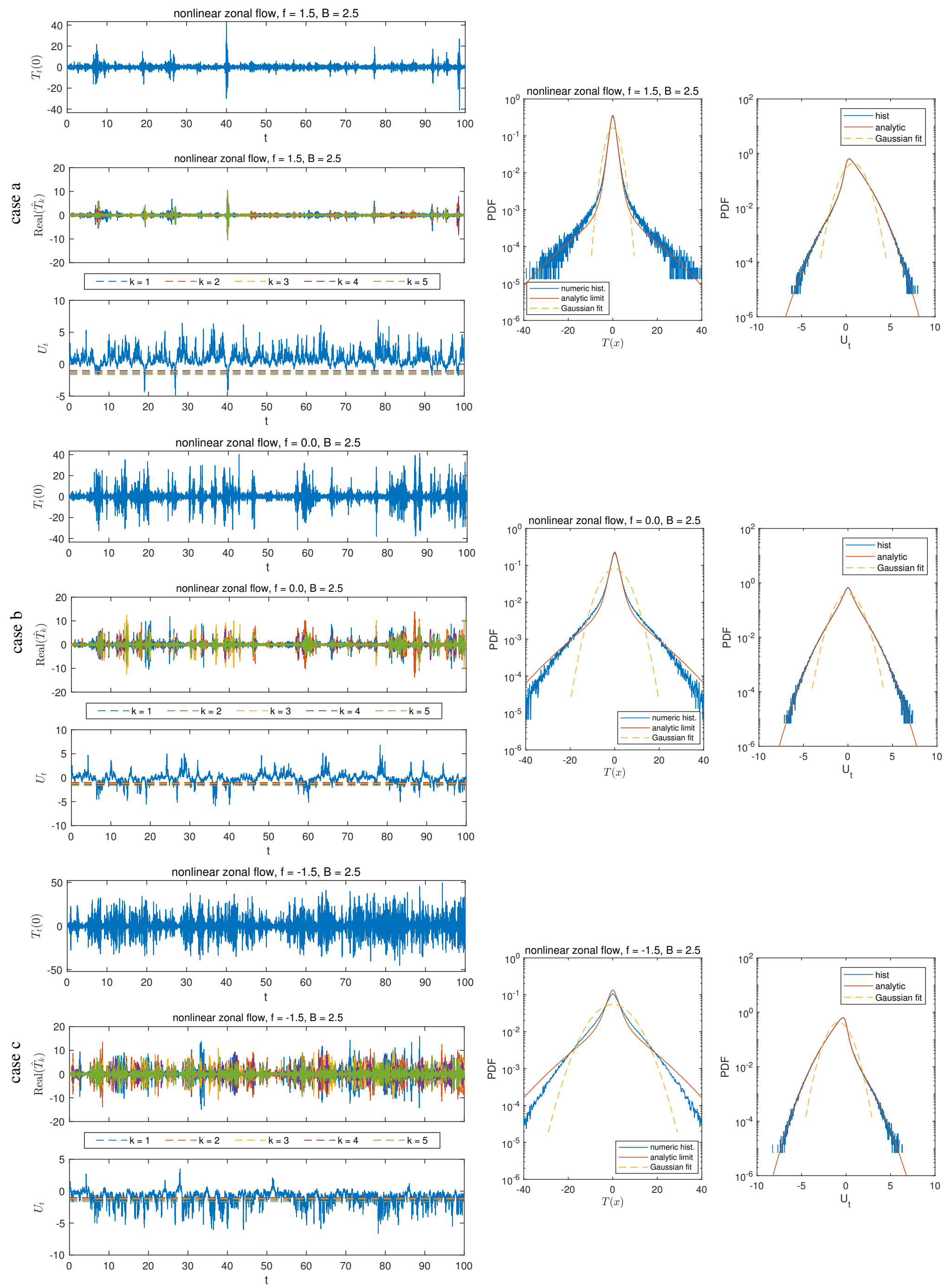

Figure 9 Multiple mode, β-plane QG flow. Nonlinear zonal fluctuations with multiplicative noise and equipartition shear spectrum.

For the shear flow we focus on a **equipartition** energy spectrum. We compare **random** shear flows,

$$\frac{\partial v_t}{\partial t} = -\gamma_v\left(\frac{\partial}{\partial x}\right)v_t + \dot{W}_v(x,t), \tag{70}$$

and **wavelike, advective** flows with

$$\frac{\partial v_t}{\partial t} = U_t R_1\left(\frac{\partial}{\partial x}\right)v_t + R_2\left(\frac{\partial}{\partial x}\right)v_t - \gamma_v\left(\frac{\partial}{\partial x}\right)v_t + \dot{W}_v(x,t), \tag{71}$$

where the wavelike operators R_1, R_2 are non zero:

$$R_1\left(\frac{\partial}{\partial x}\right) = ia_k e^{ikx}, \qquad R_2\left(\frac{\partial}{\partial x}\right) = ib_k e^{ikx}, \tag{72}$$

which encompasses **dispersive** and **non-dispersive waves**. As examples, for non-dispersive waves we have $a_k = 0$ and $b_k = -ck$ and dispersive waves include the QG baroclinic flow model. We summarize the shear models we consider and their resonance conditions below,

- Random shear flows (with zonal mean $\overline{u_r}$):

$$a_k = b_k = 0, \qquad \omega^* = -\overline{u_r}. \tag{73}$$

- Non-dispersive waves (with zonal mean $\overline{u}$):

$$a_k = 0, \quad b_k = -ck, \qquad \omega^* = c - \overline{u}. \tag{74}$$

- Dispersive waves, β-plane Quasi-Geostrophic (QG) baroclinic 1.5 layer flows (with zonal mean $\overline{u}$):

$$a_k = \frac{-k^3}{k^2+F}, \quad b_k = \frac{\beta k}{k^2+F}, \qquad \omega_k^* = -\frac{b_k + k\overline{u}}{a_k + k}. \tag{75}$$

For comparison purposes, we match the main resonance levels, between the three cases models above. For the QG model the parameters are

$$\beta = 8.91, \quad F = 16, \tag{76}$$

so when $\overline{u} = 1$, we require $c = -0.6194$ for the non-dispersive model to match the resonance level of the first mode ω_1^* in the QG model. In the purely random flow where $a_k = b_k = 0$, we need to shift the zonal mean by the same amount, which gives $\overline{u_r} = 1.6194$. All the cases are on equal footing with respect to the resonance threshold, which allows us to fairly compare the various shear models. A comparison between the nonlinear zonal flow and the linear zonal flow, is not in full equivalent since the crossing rates and overall energy are not equal, as there is no evident way to enforce equality. We consider the following zonal mean cases

- Zonal flow set 1: $\overline{u_r} = 1.0, \quad \overline{u} = 0.4171, \quad c = -0.5829$
- Zonal flow set 2: $\overline{u_r} = 1.6194, \quad \overline{u} = 1.0, \quad c = -0.6194$

In section B.1 we directly compare the random and non-dispersive advection shear model for all the aforementioned cases and in section B.2 we include a comparison for between dispersive and non-dispersive wavelike shear flows.

- Dispersive flows compared to their non-dispersive counterpart have **fewer small scale spatial features**, a direct consequence of the fact that higher modes are more rare to intermittently excite; this is also reflected in lower probabilities for extreme events in the tracer pdf.
- **Nonlinear zonal flows** in 'on-off' regimes have the ability to **drastically impact advective flows** and may lead to **super extreme events that persist in time**. A consequence of the interplay between the separated resonance phases of the tracer modes and the statistical characteristics of the nonlinear zonal fluctuation dynamics.

- Advective flows compared to their random counterpart, result in more **coherent spatio-temporal extreme events** in the tracer field with prominent **oscillatory** behavior. This is a direct consequence of the non-zero wave-speed due to the advection term.
- Advective flows compared to their random counterpart, *the limiting analytical tracer pdf predictions, derived under the $\epsilon \to 0$ limit are **identical**, but the advection flow pdf has more prominent probability for intermediate magnitude fluctuations corresponding to the oscillatory behavior,* the effects are order ϵ. In very intermittent regimes, the tails of the tracer pdf in advective flows clearly follows an **exponential**-like form for the intermediate to extreme tails range.

8 Conclusion

This study reveals the critical mechanisms through which stochastic zonal and shear flows produce tracer intermittency in turbulent diffusion with a mean gradient. By making assumptions that preserve key physical mechanisms of tracer transport, following previous literature, we derived analytically tractable pathwise solutions and explicit expressions for the tracer PDF. Following this, a simplified analytical approximation was derived for the conditional variance of the tracer field, under a slowly varying velocity field, which provides a closed form equation for the tracer PDF that was validated through numerical experiments. From these analytical results and numerical experiments, we demonstrated several key velocity field features that determine how non-Gaussianity and extreme events arise in tracer fields.

The primary result reveals that resonance, through phase speed alignment between the zonal and shear flow, rather than transient instabilities, are responsible for the observed tracer intermittency. When the phase speeds of zonal flow fluctuations cross specific thresholds, determined by the underlying wave dynamics of the velocity field, dramatic amplification of tracer variance occurs. This resonance-driven mechanism represents a pathway to turbulent intermittency that differs from finite-time Lyapunov instabilities. The analytical framework demonstrates that the conditional variance of the tracer field peaks when $\omega_{R,k} = 0$, corresponding to resonance conditions between the zonal flow, shear flow, and tracer field. This provides a quantitative explanation of extreme events and allows for prediction of intermittency if the flow characteristics are known.

Importantly, we identified significant differences in tracer behavior across flow regimes. Dispersive flows with wavelike features exhibit separated resonance thresholds across wavenumbers, leading to sequential excitation of modes and smoother extreme events. In contrast, random shear flows and non-dispersive waves synchronize these thresholds, exciting all scales simultaneously, producing sharper, more intermittent, structures with enhanced small-scale features. Our comparison of equipartition and Kolmogorov energy spectra show that the spatial structure of extreme events is strongly influenced by the distribution of energy in the shear flow. Under equipartition, multiple peaks in the conditional variance lead to stronger intermittency with pronounced small-scale features, whereas the Kolmogorov spectrum produces more large-scale dominated extreme events.

The nonlinear dynamics of zonal flow is crucial in modulating intermittency. Despite being statistically non-Gaussian, nonlinear zonal flows do not necessarily enhance tracer intermittency; rather, their effect depends on how frequently they cross resonance thresholds. This challenges linearization approaches and highlights the importance of accurately capturing zonal flow statistics in turbulent transport models.

The results in this paper have implications for modeling and prediction of tracer transport in geophysical and environmental applications. The identified resonance mechanism provides a simple basis for understanding tracer bursts in systems ranging from atmospheric pollutant transport to oceanic mixing. Furthermore, the demonstrated sensitivity to flow characteristics shows that accurate representation of zonal and shear flow statistics is essential for reliable prediction of extreme tracer burst events. Future work could extend this approach to three-dimensional flows involving a vertical shear and use the model in various data assimilation (DA) and uncertainty quantification (UQ) applications. The analytical tractability of our approach makes it particularly valuable for developing and testing various DA and UQ schemes that can capture non-Gaussian statistics of tracer intermittency while remaining computationally efficient.

Acknowledgments

M.A.M is partially supported by NSERC Discovery Grant and Alberta Innovates. D. Q. is partially supported by ONR Grant N00014-24-1-2192, and NSF Grant DMS-2407361. The authors would also like to dedicate this paper to the memory of Andrew J. Majda whose contributions made this work possible.

References

[1] A. Bourlioux and A. J. Majda. "Elementary Models with Probability Distribution Function Intermittency for Passive Scalars with a Mean Gradient". In: *Physics of Fluids* 14.2 (Feb. 1, 2002), pp. 881–897.

[2] N. Chen and A. J. Majda. "Filtering Nonlinear Turbulent Dynamical Systems through Conditional Gaussian Statistics". In: *Monthly Weather Review* 144.12 (Dec. 1, 2016), pp. 4885–4917.

[3] S. Janson. *Roots of Polynomials of Degrees 3 and 4*. Sept. 13, 2010. URL: http://arxiv.org/abs/1009.2373. Pre-published.

[4] A. N. Kolmogorov. "The Local Structure of Turbulence in Incompressible Viscous Fluid for Very Large Reynolds". In: *Numbers. In Dokl. Akad. Nauk SSSR* 30 (1941), p. 301.

[5] R. S. Liptser and A. N. Shiryaev. *Statistics of Random Processes II. Applications*. 2nd ed. Stochastic Modelling and Applied Probability 6. Springer-Verlag Berlin Heidelberg, 2001.

[6] A. Majda. *Introduction to PDEs and Waves for the Atmosphere and Ocean*. Courant Lecture Notes in Mathematics 9. New York : Providence, R.I: Courant Institute of Mathematical Sciences ; American Mathematical Society, 2003. 234 pp.

[7] A. J. Majda and X. T. Tong. "Intermittency in Turbulent Diffusion Models with a Mean Gradient". In: *Nonlinearity* 28.11 (Oct. 1, 2015), pp. 4171–4208.

[8] A. J. Majda, C. Franzke, and D. Crommelin. "Normal Forms for Reduced Stochastic Climate Models". In: *Proceedings of the National Academy of Sciences* 106.10 (Mar. 10, 2009), pp. 3649–3653.

[9] A. J. Majda and B. Gershgorin. "Elementary Models for Turbulent Diffusion with Complex Physical Features: Eddy Diffusivity, Spectrum and Intermittency". In: *Philosophical Transactions of the Royal Society A: Mathematical, Physical and Engineering Sciences* 371.1982 (Jan. 13, 2013), p. 20120184.

[10] A. J. Majda and P. R. Kramer. "Simplified Models for Turbulent Diffusion: Theory, Numerical Modelling, and Physical Phenomena". In: *Physics Reports* 314.4–5 (June 1999), pp. 237–574.

[11] Marco Avellaneda and A. J. Majda. "Simple Examples with Features of Renormalization for Turbulent Transport". In: *Philosophical Transactions of the Royal Society of London. Series A: Physical and Engineering Sciences* 346.1679 (Feb. 15, 1994), pp. 205–233.

[12] J. D. Neelin, B. R. Lintner, B. Tian, Q. Li, L. Zhang, P. K. Patra, M. T. Chahine, and S. N. Stechmann. "Long Tails in Deep Columns of Natural and Anthropogenic Tropospheric Tracers". In: *Geophysical Research Letters* 37.5 (Mar. 1, 2010).

[13] L. F. Richardson. "Atmospheric Diffusion Shown on a Distance-Neighbour Graph". In: *Proceedings of the Royal Society of London. Series A, Containing Papers of a Mathematical and Physical Character* 110.756 (Apr. 1926), pp. 709–737.

[14] K. R. Sreenivasan. "Turbulent Mixing: A Perspective". In: *Proceedings of the National Academy of Sciences* 116.37 (Sept. 10, 2019), pp. 18175–18183.

[15] G. I. Taylor. "Diffusion by Continuous Movements". In: *Proceedings of the London Mathematical Society* s2-20.1 (1922), pp. 196–212.

[16] G. K. Vallis. *Atmospheric and Oceanic Fluid Dynamics: Fundamentals and Large-Scale Circulation*. Cambridge: Cambridge university press, 2006.

[17] Z. Warhaft. "Passive Scalars in Turbulent Flows". In: *Annual Review of Fluid Mechanics* 32 (Volume 32, 2000 Jan. 1, 2000), pp. 203–240.

[18] Y. Yuan and A. J. Majda. "Invariant Measures and Asymptotic Gaussian Bounds for Normal Forms of Stochastic Climate Model". In: *Chinese Annals of Mathematics, Series B* 32.3 (May 2011), pp. 343–368.

A Supporting information

A.1 Dynamical regimes of the nonlinear zonal flow

To study the dynamical regimes of the nonlinear cross sweep model in eq. (32) we consider the deterministic system with no noise and study its fixed points:

$$\frac{dx}{dt} = f + ax + bx^2 - cx^3. \tag{A.1}$$

The three roots of the cubic equation $f + ax + bx^2 - cx^3 = 0$ determine the equilibrium points. With $c > 0$ it is straightforward to see we have three possible regimes corresponding to the nature of the three roots of the cubic: two stable and one unstable fixed points, one stable and one unstable fixed points, or one stable fixed point and two non-real complex conjugate roots. The parameters a, b, c, f determine the nature of the roots of the cubic polynomial through the discriminant. For the cubic polynomial in standard form,

$$f(x) = x^3 + c_2x^2 + c_1x + c_0, \tag{A.2}$$

the discriminant is given by [3]

$$\Delta = c_2^2c_1^2 - 4c_1^3 - 4c_2^3c_0 + 18c_2c_1c_0 - 27c_0^2 \tag{A.3}$$

$$= -4p^3 - 27q^2, \quad \text{where } p = c_1 - \tfrac{1}{3}c_2^2, \quad q = c_0 - \tfrac{1}{3}c_2c_1 + \tfrac{2}{27}c_2^3. \tag{A.4}$$

The boundary between the three possible cases is given by the condition $\Delta = 0$. The form for the discriminant in eq. (A.4) allows us to explicitly determine the boundaries separating the different cases by setting the discriminant to zero $\Delta = 0$ and solving for c_0. In terms of the original system parameters, this gives the following equation for the boundary as a function of the other parameters

$$f_b^{\pm} = -\frac{ab}{3c} - \frac{2b^3}{27c^2} \pm 2c\left(\frac{a}{3c} + \frac{b^2}{9c^2}\right)^{3/2}, \tag{A.5}$$

where we require $a > a_c \equiv -b^2/3c$, for $c > 0$. Given fixed c and b, this boundary divides the dynamics in the parameter space (a, f) into two regimes: a region with three equilibrium points (two stable and one unstable) when $f_b^- < f < f_b^+$ and $a > a_c$ and the region outside this area with only one stable equilibrium point, see fig. A.1.

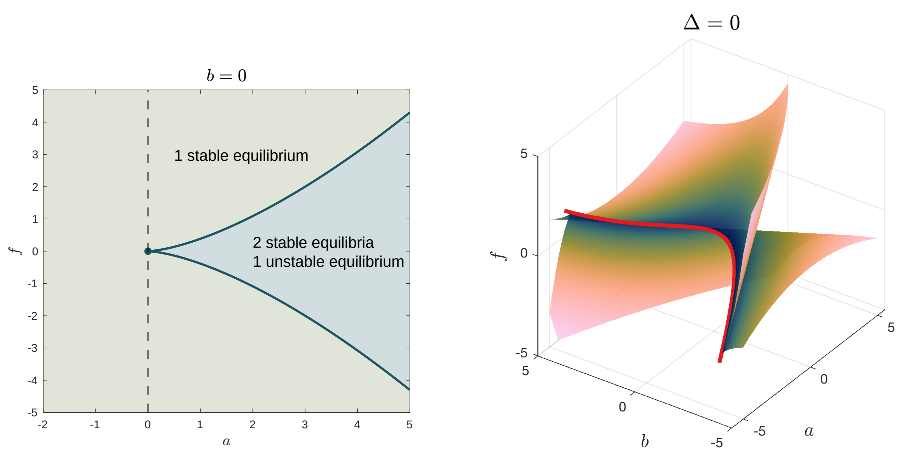

Figure A.1 Regimes of the deterministic nonlinear cubic model in (a, f) parameter space for $b = 0$ values (left panel). The dark shaded area is bounded by the dividing curve $f_b^{\pm}$ in eq. (A.5) with points on the boundary having one unstable and one stable fixed points. Boundary for the discriminant $\Delta = 0$ is shown in the right panel.

A.2 Equilibrium density of the nonlinear zonal flow

The stationary probability measure for the general form of the nonlinear zonal flow in eq. (32) satisfies the following Fokker-Planck equation

$$-\frac{\partial}{\partial x}[\left(ax+bx^2-cx^3+f\right)p_U(x)]+\frac{1}{2}\frac{\partial^2}{\partial x^2}[\left((Bx-A)^2+\sigma_u^2\right)p_U(x)]=0 \tag{A.6}$$

The equilibrium pdf that solves this can be shown to given by (see [18] for details)

$$p_u(u)=\frac{N_0}{((Bx-A)^2+\sigma_u^2)^{a_1}}\exp\left(d\arctan\left(\frac{Bx-A}{\sigma_u}\right)\right)\exp\left(\frac{-c_1x^2+b_1x}{B^4}\right), \tag{A.7}$$

where N_0 is a normalization constant. The coefficients a_1, b_1, c_1, d are provided in .

$$a_1=1-\frac{-3A^2c+aB^2+2AbB+c\sigma_u^2}{B^4}, \tag{A.8}$$
$$b_1=2bB^2-4cAB, \tag{A.9}$$
$$c_1=cB^2, \tag{A.10}$$
$$d=\frac{d_1}{\sigma_u}+d_2\sigma_u, \tag{A.11}$$
$$d_1=2\frac{A^2bB-A^3c+AaB^2+B^3f}{B^4}, \tag{A.12}$$
$$d_2=2\frac{3cA-bB}{B^4}. \tag{A.13}$$

A.3 Proofs of major results

Proposition 3.1. Integrating the equation for $\widehat{T}_{k,t}$ by using eq. (37) we find

$$\begin{aligned}\widehat{T}_{k,t}&=-\alpha\int_0^t\exp(-\gamma_{T,k}(t-s)+i\omega_{T,k}[s,t])\hat{v}_{k,s}\,ds &\text{(A.14)}\\ &=-\alpha\sigma_{v,k}\int_0^t\int_0^s\exp(-\gamma_{T,k}(t-s)-\gamma_{v,k}(s-r)++i\omega_{T,k}[s,t]+i\omega_{v,k}[r,s])\,dB_{k,r}\,ds &\text{(A.15)}\\ &=-\alpha\sigma_{v,k}\int_0^t\int_r^t\exp(-\gamma_{T,k}(t-s)-\gamma_{v,k}(s-r)++i\omega_{T,k}[s,t]+i\omega_{v,k}[r,s])\,ds\,dB_{k,r}. &\text{(A.16)}\end{aligned}$$

Fubini's theorem is used in the last equality to exchange the order of integration.

Proposition 3.2. The derivation of the variance of trajectory solutions conditioned on a zonal flow trajectory is given by

$$\begin{aligned}\Sigma_{k,t|u}&=\alpha^2\sigma_{v,k}^2\int_0^t\left|\int_r^t\exp(-\gamma_{T,k}(t-s)-\gamma_{v,k}(s-r)++i\omega_{T,k}[s,t]+i\omega_{v,k}[r,s])\,ds\right|^2dr &\text{(A.17)}\\ &=\alpha^2\sigma_{v,k}^2\int_0^t\left|\int_r^t\exp(-\gamma_{T,k}t+\gamma_{v,k}r+\gamma_{R,k}s+i\omega_{T,k}[s,t]+i\omega_{v,k}[r,t]-i\omega_{v,k}[s,t]))\,ds\right|^2dr &\text{(A.18)}\\ &=\alpha^2\sigma_{v,k}^2\int_0^t\left|\int_r^t\exp(-\gamma_{T,k}t+\gamma_{v,k}r+i\omega_{v,k}[r,t]+\gamma_{R,k}s+i\omega_{R,k}[s,t]\,ds\right|^2dr &\text{(A.19)}\\ &=\alpha^2\sigma_{v,k}^2\int_0^t\left|\exp(-\gamma_{T,k}t+\gamma_{v,k}r+i\omega_{v,k}[r,t])\int_r^t\exp(\gamma_{R,k}s+i\omega_{R,k}[s,t])\,ds\right|^2dr &\text{(A.20)}\\ &=\alpha^2\sigma_{v,k}^2\int_0^t\exp(-2\gamma_{T,k}t+2\gamma_{v,k}r)\left|\int_r^t\exp(\gamma_{R,k}s+i\omega_{R,k}[s,t])\,ds\right|^2dr, &\text{(A.21)}\end{aligned}$$

where $\omega_{R,k} \coloneqq \omega_{T,k} - \omega_{v,k} = -(a_k + k)u_t - b_k$ and $\gamma_{R,k} \coloneqq \gamma_{T,k} - \gamma_{v,k}$. Alternatively, we can express the variance as:

$$\Sigma_{k,t|u} = \alpha^2\sigma_{v,k}^2 \int_0^t \exp(-2\gamma_{v,k}(t-r)) \left| \int_r^t \exp(-\gamma_{R,k}(t-s) + i\omega_{R,k}[s,t])\, ds \right|^2 dr. \tag{A.22}$$

Corollary 3.3. We can find an upper bound for the conditional variance as follows. Start from eq. (42) and first use $|\int z| \le \int |z| = \int r$, where $z = re^{i\theta}$, for the inner integral to obtain:

$$\left| \int_r^t \exp(\gamma_{R,k}s + i\omega_{R,k}[s,t])\, ds \right|^2 \le \left(\int_r^t e^{\gamma_R s}\, ds \right)^2 = \frac{1}{\gamma_R^2}(e^{\gamma_R t} - e^{\gamma_R r})^2 \le \frac{1}{\gamma_R^2}(e^{2\gamma_R t} + e^{2\gamma_R r}), \tag{A.23}$$

$$\Sigma_{k,t|u} = \alpha^2\sigma_{v,k}^2 \int_0^t \exp(-2\gamma_{T,k}t + 2\gamma_{v,k}r) \left| \int_r^t \exp(\gamma_{R,k}s + i\omega_{R,k}[s,t])\, ds \right|^2 dr \tag{A.24}$$

$$\le \alpha^2\sigma_{v,k}^2 \int_0^t \exp(-2\gamma_{T,k}t + 2\gamma_{v,k}r) \frac{1}{\gamma_{R,k}^2}(e^{2\gamma_{R,k}t} + e^{2\gamma_{R,k}r})\, dr \tag{A.25}$$

$$= \alpha^2\sigma_{v,k}^2 \int_0^t \frac{1}{\gamma_{R,j}^2}(e^{-2\gamma_{v,k}(t-r)} + e^{-2\gamma_{T,k}(t-r)})\, dr \tag{A.26}$$

$$= \frac{\alpha^2\sigma_{v,k}^2}{\gamma_{R,k}^2}\left(\frac{1 - e^{-2\gamma_{v,k}t}}{2\gamma_{v,k}} + \frac{1 - e^{-2\gamma_{T,k}t}}{2\gamma_{T,k}} \right) \tag{A.27}$$

We also find the bound in the long time limit

$$\lim_{t\to\infty} \Sigma_{k,t|u} \le \frac{\alpha^2\sigma_{v,k}^2}{\gamma_{R,k}^2}\left(\frac{1}{2\gamma_{v,k}} + \frac{1}{2\gamma_{T,k}} \right) \tag{A.28}$$

Proposition 4.2. Starting from eq. (A.22) for the rescaled system in definition 4.1,

$$\Sigma_{k,t|u} = \epsilon^{-2}\alpha^2\sigma_{v,k}^2 \int_0^t \exp(-2\gamma_{v,k}(t-r)) \left| \int_r^t \exp(-\gamma_{R,k}(t-s) + i\epsilon^{-1}\omega_{R,k}[s,t])\, ds \right|^2 dr, \tag{A.29}$$

where $\gamma_{R,k} = \epsilon^{-1}\gamma_{T,k} - \gamma_{v,k}$. Define the inner integral

$$I(r) \coloneqq \int_r^t \exp\Big(-(\epsilon^{-1}\gamma_{T,k} - \gamma_{v,k})(t-s) + i\epsilon^{-1}\omega_{R,k}[s,t]\Big)\, ds, \tag{A.30}$$

where $\omega_{R,k}[s,t] = \int_s^t \omega_{R,k}(u)\, du$. Consider the change of variables $u = t - s$,

$$I(r) = \int_0^{t-r} \exp\Big(-\epsilon^{-1}\gamma_{T,k}u\Big) \exp\Big(\gamma_{v,k}u + i\epsilon^{-1}\omega_{R,k}[t-u,t]\Big)\, du, \tag{A.31}$$

In the small ϵ limit, most of the contribution to this integral comes from when u is small. As a result $\omega_{R,k}[t-u,t] \approx \omega_{R,k}(t)u$:

$$I(r) \approx \int_0^{t-r} \exp\big(\epsilon^{-1}(-\gamma_{T,k} + i\omega_{R,k}(t))u\big)\, du, \tag{A.32}$$

This integral is of the form

$$\int_0^{t-r} \exp(-\lambda u) du = \frac{1}{\lambda}(1 - \exp(-\lambda(t-r))), \quad \text{where } \lambda = \epsilon^{-1}(\gamma_{T,k} - i\omega_{R,k}(t) \tag{A.33}$$

Taking the modulus square and keeping only leading order terms we find

$$|I(r)|^2 \approx \frac{\epsilon^2}{\gamma_{T,k}^2 + \omega_{R,k}(t)^2}. \tag{A.34}$$

Using this result in eq. (A.29) we obtain

$$\Sigma_{k,t|u} = \epsilon^{-2}\alpha^2\sigma_{v,k}^2 \int_0^t \exp(-2\gamma_{v,k}(t-r)) \frac{\epsilon^2}{\gamma_{T,k}^2 + \omega_{R,k}(t)^2}\, dr \tag{A.35}$$

$$= \frac{\alpha^2\sigma_{v,k}^2}{2\gamma_{v,k}\left(\gamma_{T,k}^2 + \omega_{R,k}(t)^2\right)}\left(1 - \exp(-2\gamma_{v,k}t)\right). \tag{A.36}$$

As $t \to \infty$, the conditional variance $\Sigma_{k,t|u}$ converges to the stationary value

$$\tilde{\Sigma}_k(u) = \frac{\alpha^2 E_{v,k}}{\gamma_{T,k}^2 + \omega_{R,k}(u)^2}, \quad \text{where } E_{v_k} = \frac{\sigma_{v,k}^2}{2\gamma_{k,v}}. \tag{A.37}$$

B Experiments

B.1 Side-by-side comparison of random and advective flow (non-dispersive)

Set 1: Figures B.2 to B.4
Set 2: Figures B.8 to B.10

B.2 Side-by-side comparison of non-dispersive and dispersive advective flows

Set 1: Figures B.5 and B.7
Set 2: Figures B.11 to B.13

zonal flow set 1: $\overline{u_r} = 1.0, \quad \overline{u} = 0.4171, \quad c = -0.5829$

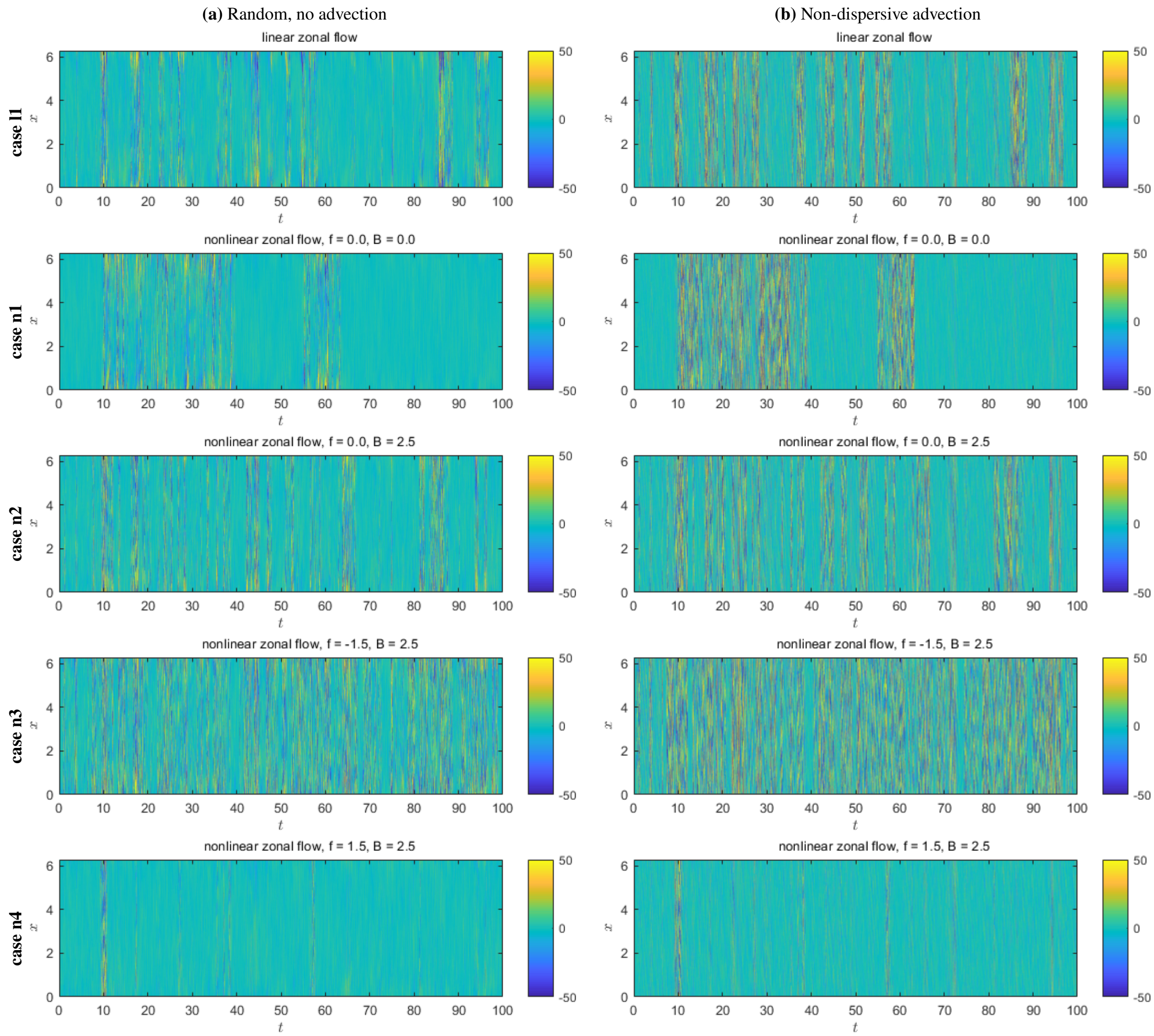

Figure B.2 Comparison of spatio-temporal evolution of the tracer field, under different shear flow models, for **equipartition**.

zonal flow set 1: $\overline{u_r} = 1.0, \quad \overline{u} = 0.4171, \quad c = -0.5829$

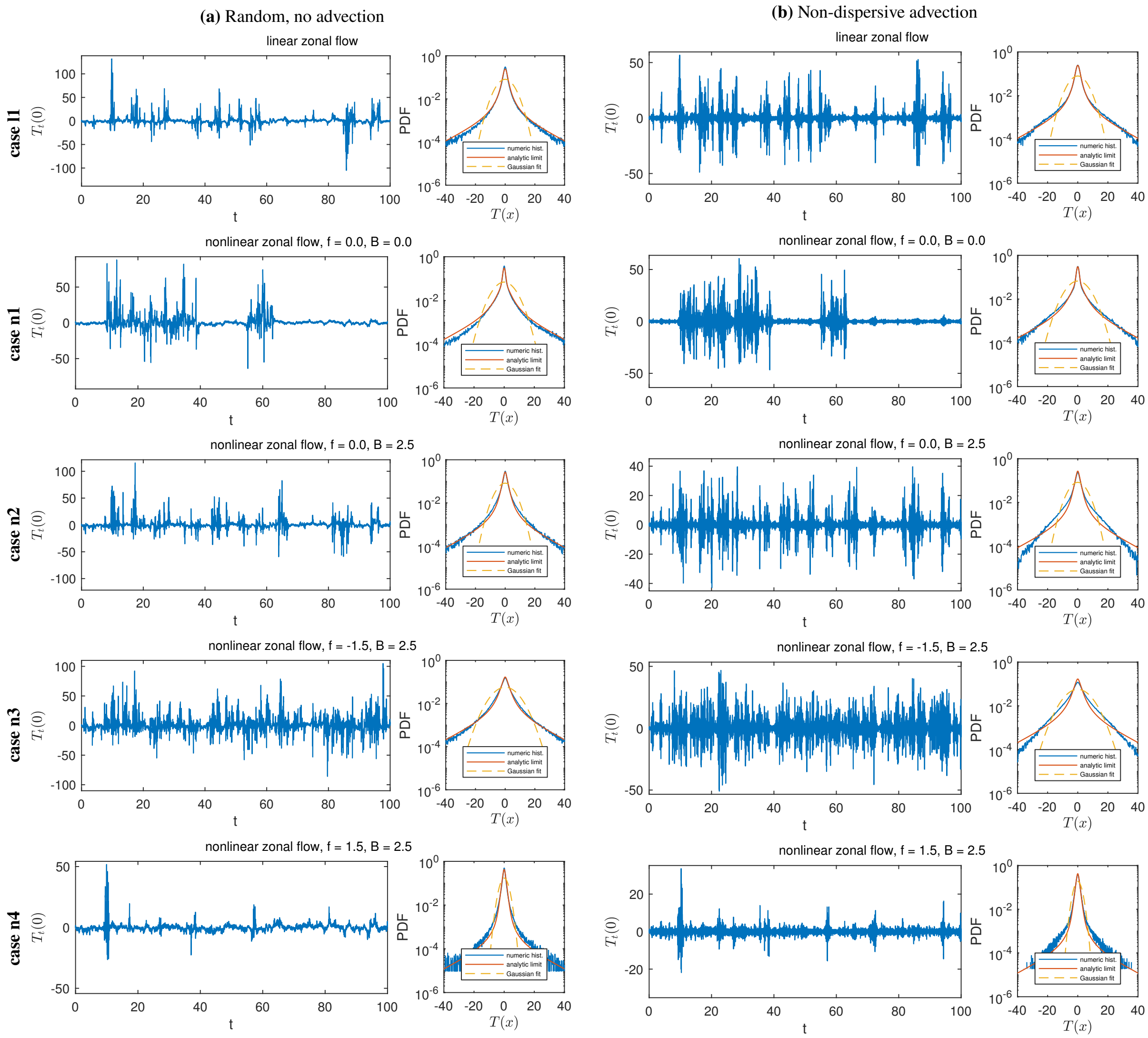

Figure B.3 Comparison of evolution of the tracer field at $T_t(0)$ and the stationary PDF, among different shear flow models.

zonal flow set 1: $\overline{u_r} = 1.0, \quad \overline{u} = 0.4171, \quad c = -0.5829$

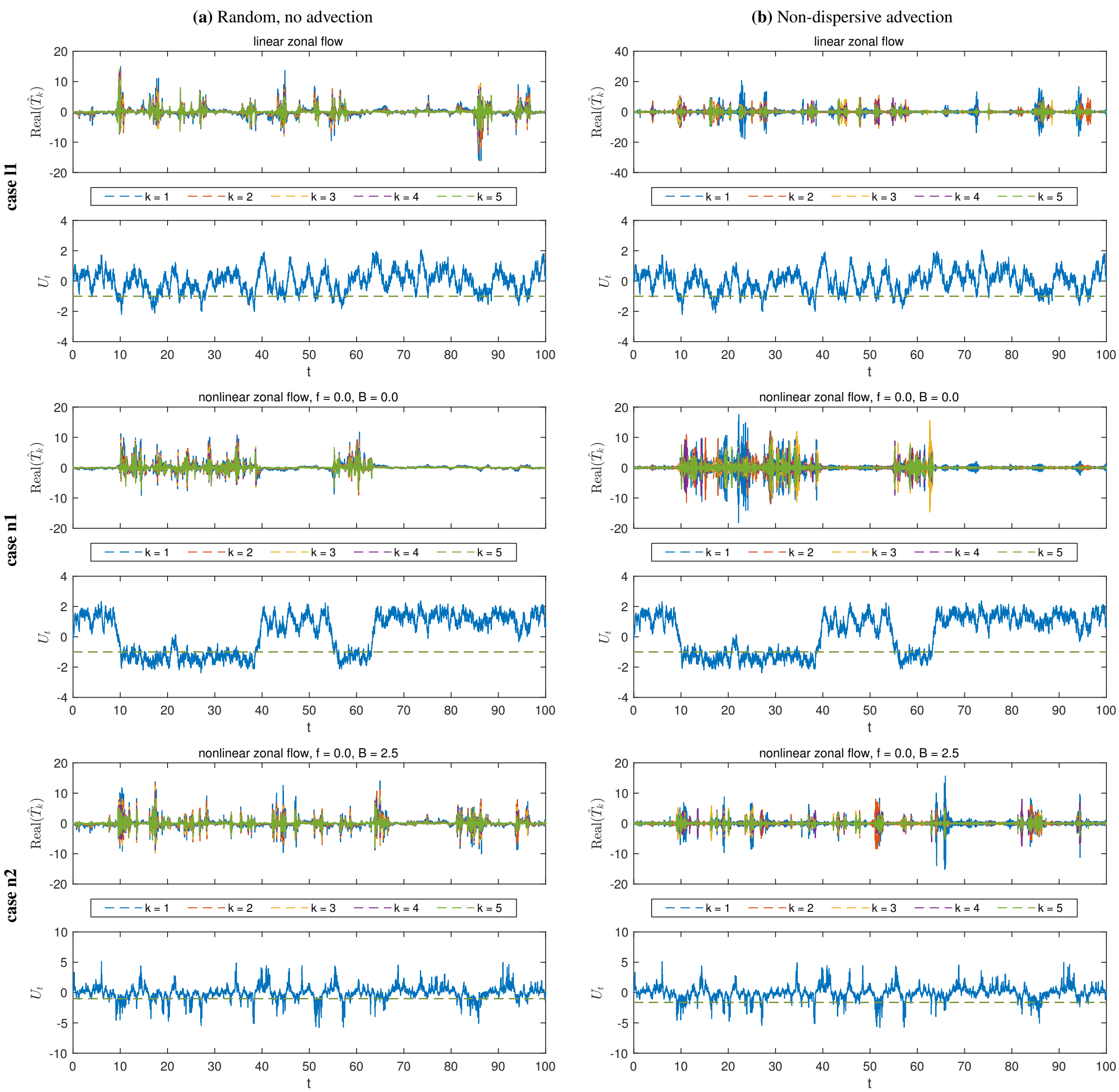

Figure B.4 Comparison of evolution of the tracer modes and zonal fluctuation.

zonal flow set 1: $\overline{u_r} = 1.0, \quad \overline{u} = 0.4171, \quad c = -0.5829$

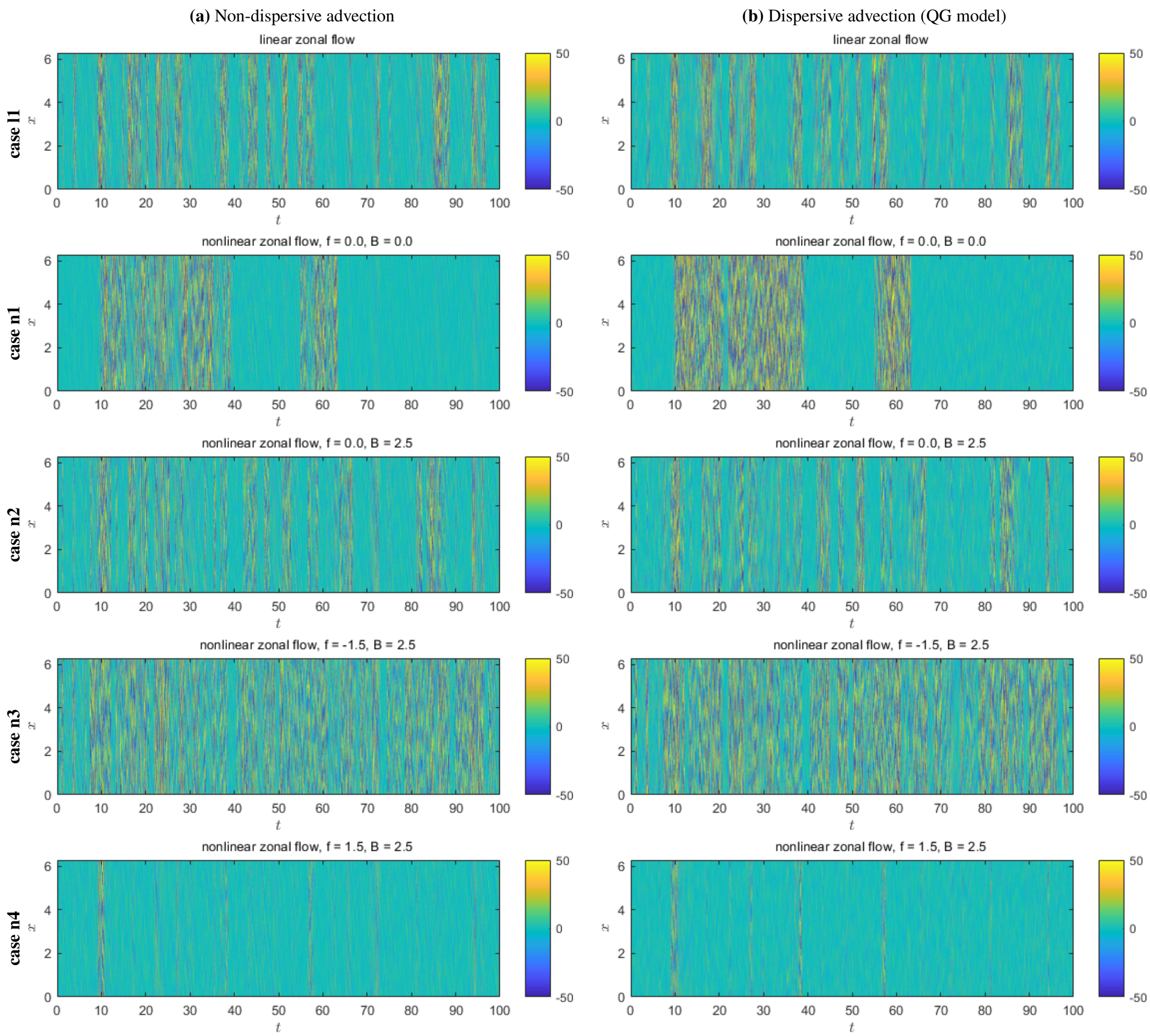

Figure B.5 Comparison of spatio-temporal evolution of the tracer field, under different shear flow models, for **equipartition**.

zonal flow set 1: $\overline{u_r} = 1.0, \quad \overline{u} = 0.4171, \quad c = -0.5829$

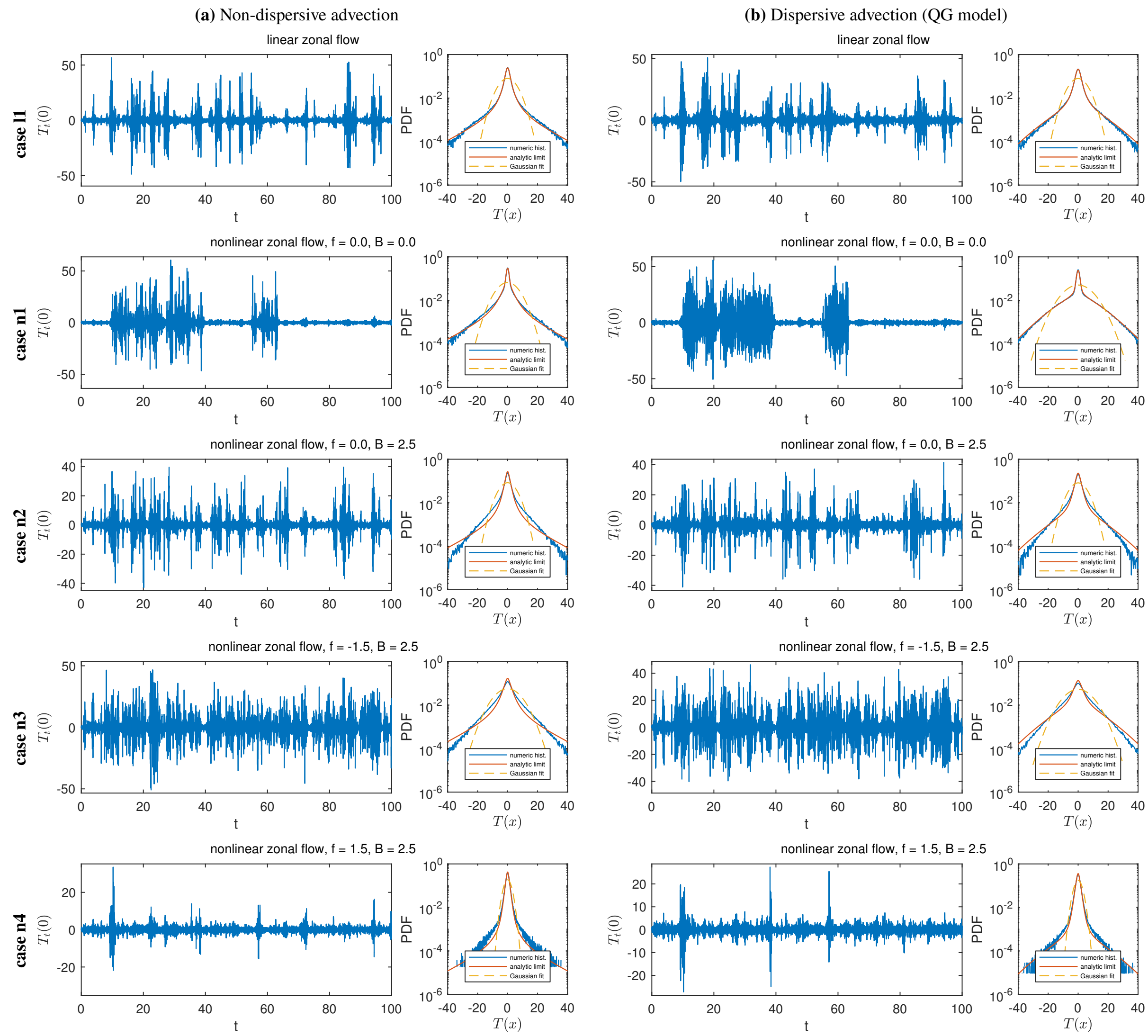

Figure B.6 Comparison of evolution of the tracer field at $T_t(0)$ and the stationary PDF, among different shear flow models.

zonal flow set 1: $\overline{u_r} = 1.0, \quad \overline{u} = 0.4171, \quad c = -0.5829$

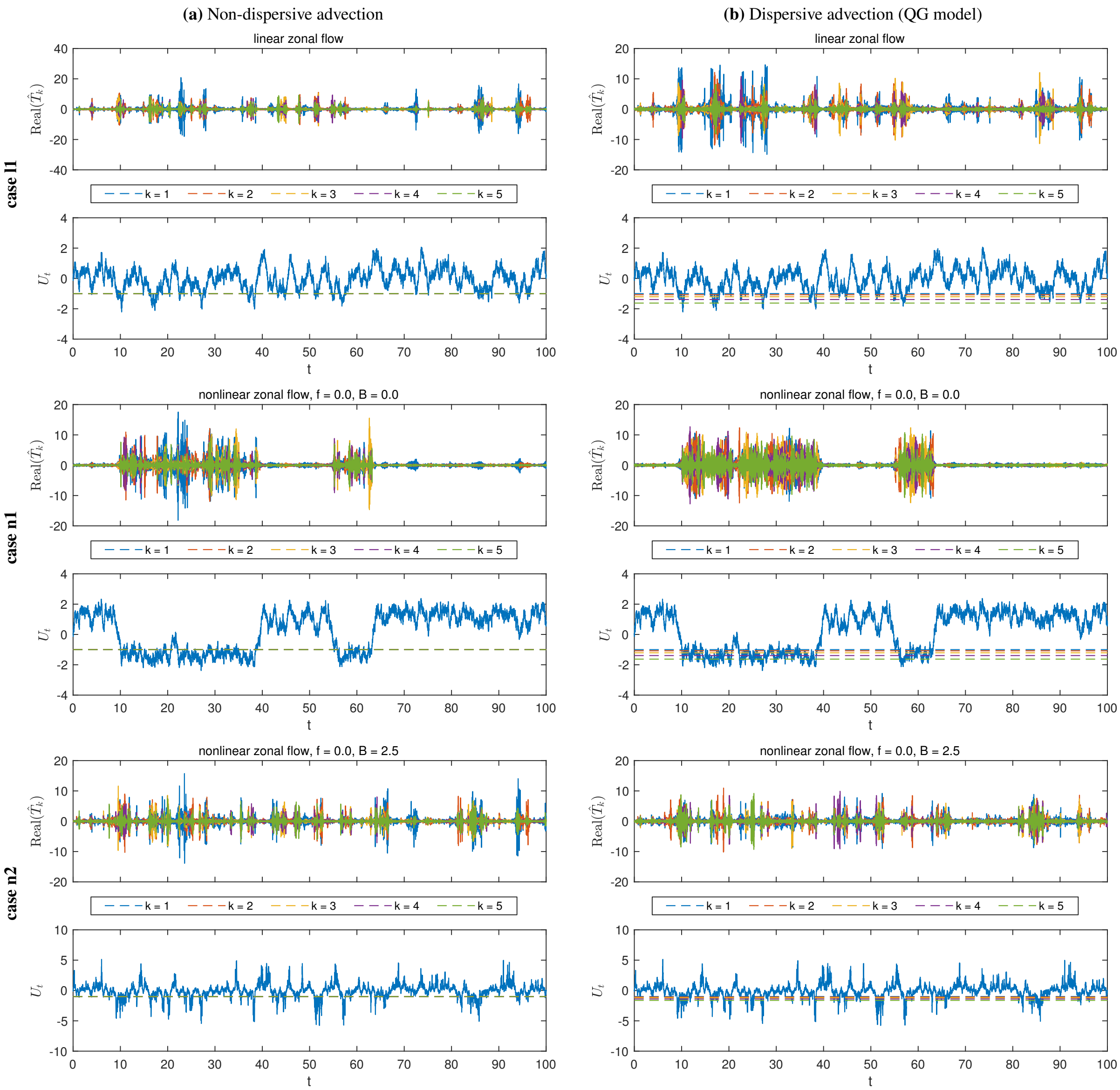

Figure B.7 Comparison of evolution of the tracer modes and zonal fluctuation.

zonal flow set 2: $\overline{u_r} = 1.6194, \quad \overline{u} = 1.0, \quad c = -0.6194$

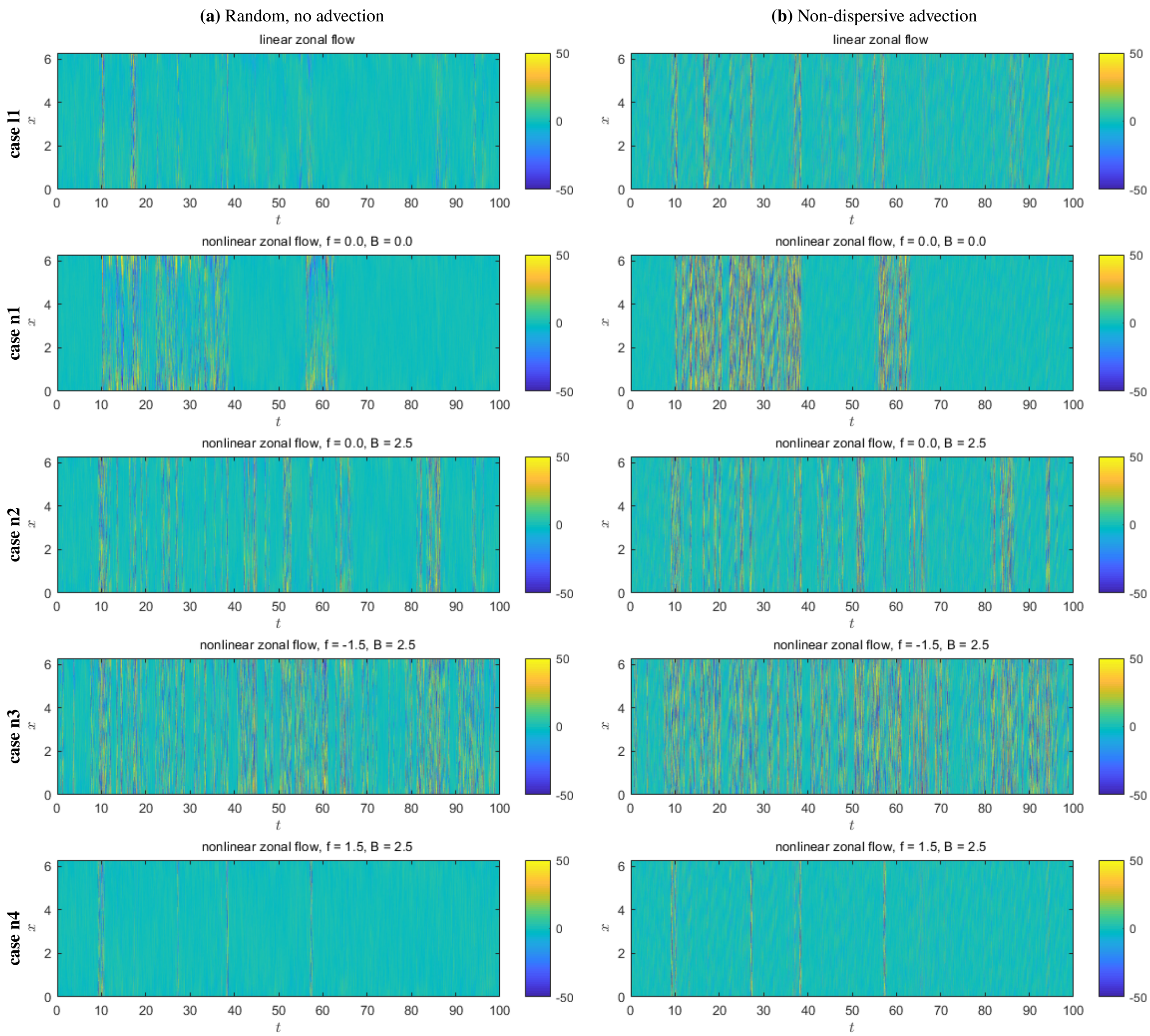

Figure B.8 Comparison of spatio-temporal evolution of the tracer field, under different shear flow models, for **equipartition**.

zonal flow set 2: $\overline{u_r} = 1.6194, \quad \overline{u} = 1.0, \quad c = -0.6194$

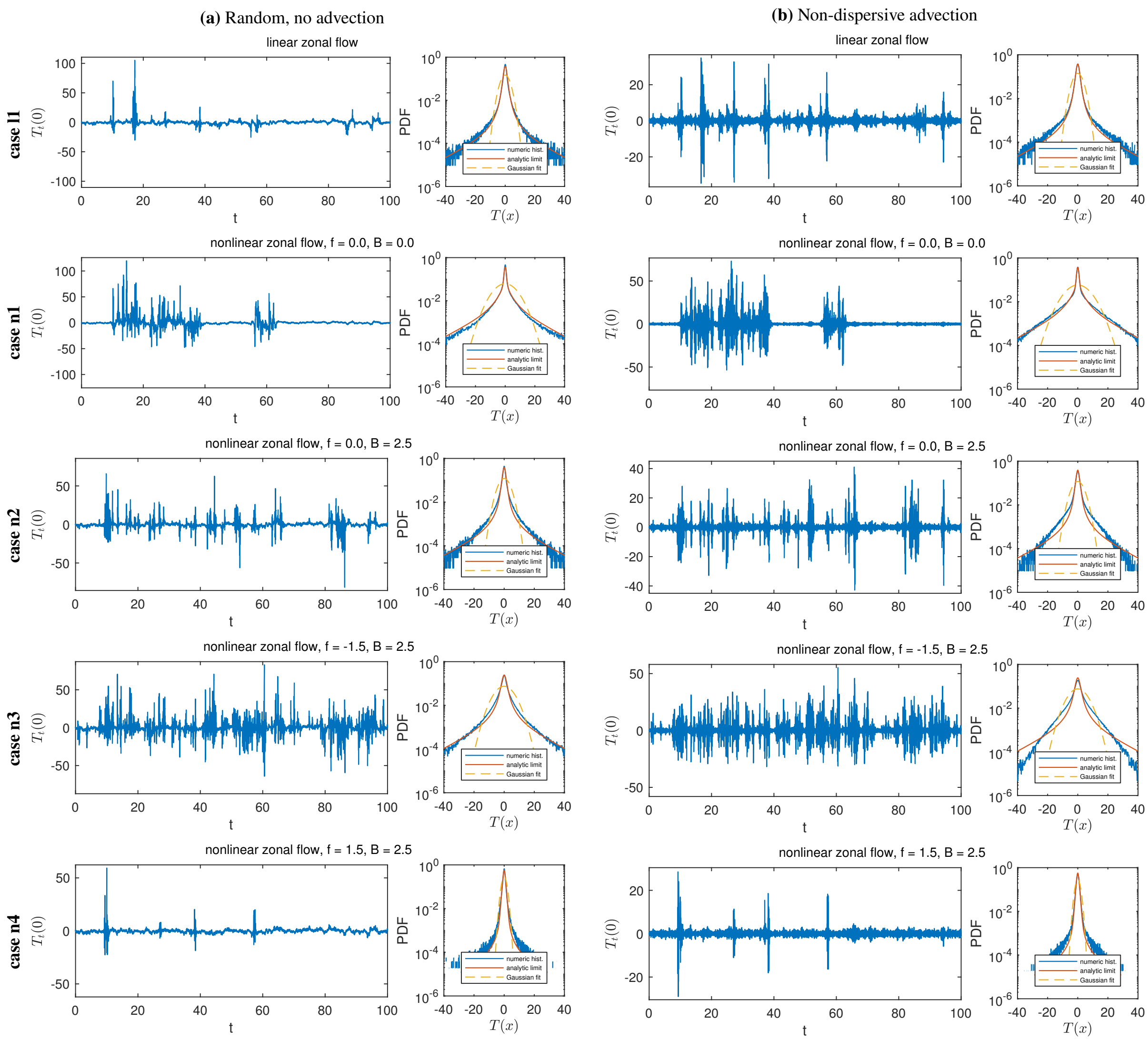

Figure B.9 Comparison of evolution of the tracer field at $T_t(0)$ and the stationary PDF, among different shear flow models.

zonal flow set 2: $\overline{u_r} = 1.6194, \quad \overline{u} = 1.0, \quad c = -0.6194$

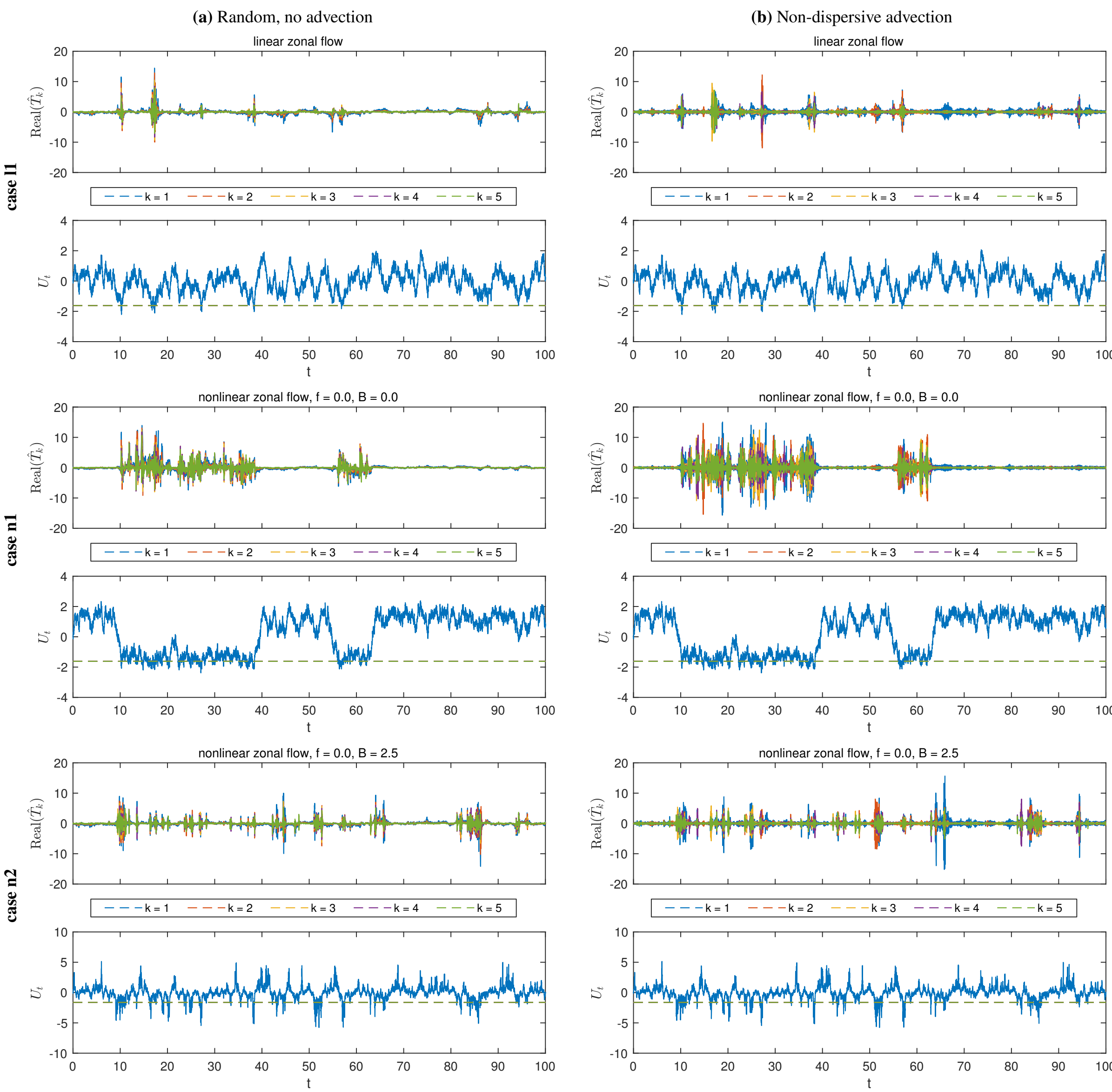

Figure B.10 Comparison of evolution of the tracer modes and zonal fluctuation.

zonal flow set 2: $\overline{u_r} = 1.6194, \quad \overline{u} = 1.0, \quad c = -0.6194$

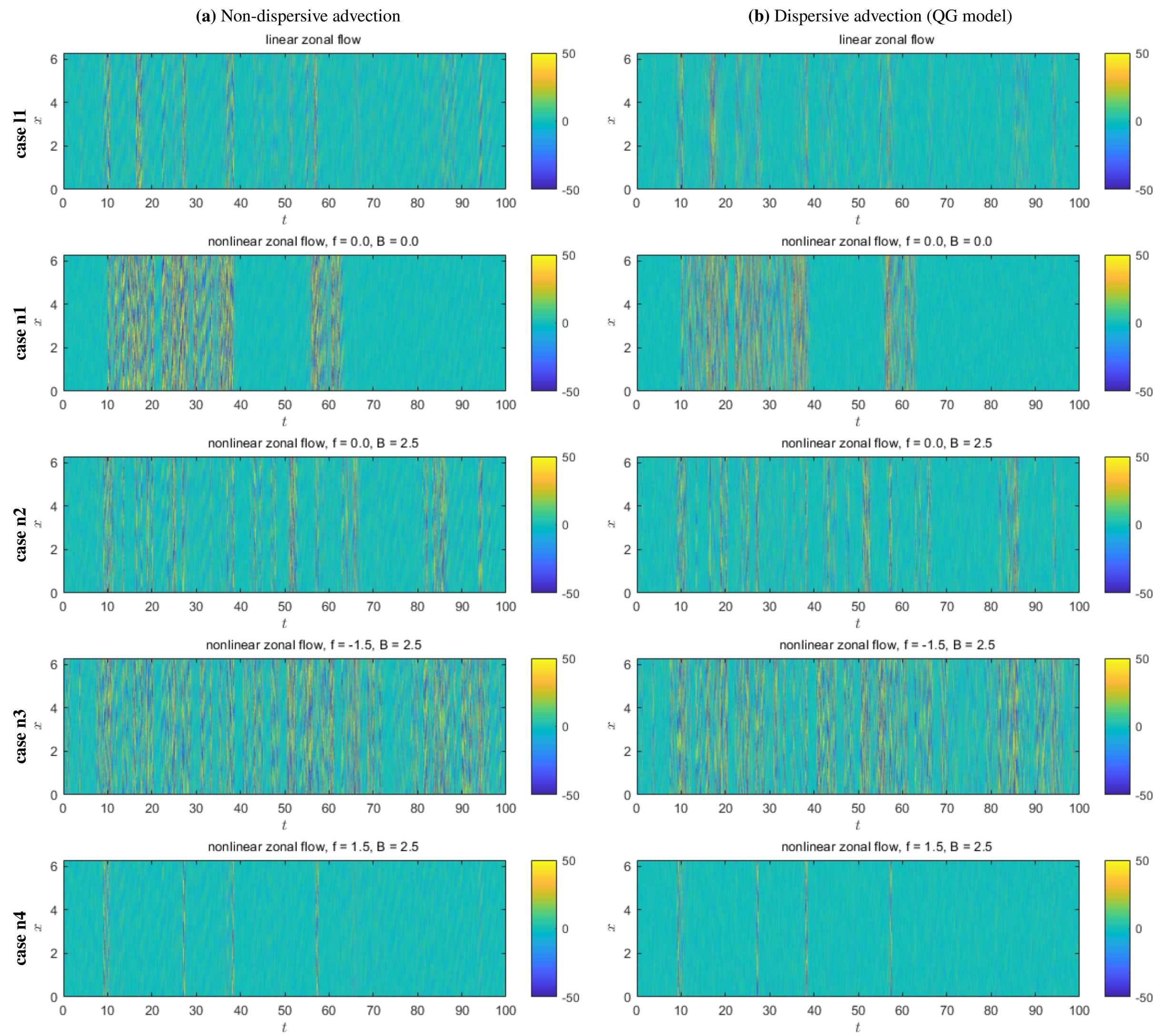

Figure B.11 Comparison of spatio-temporal evolution of the tracer field, under different shear flow models, for **equipartition**.

zonal flow set 2: $\overline{u_r} = 1.6194, \quad \overline{u} = 1.0, \quad c = -0.6194$

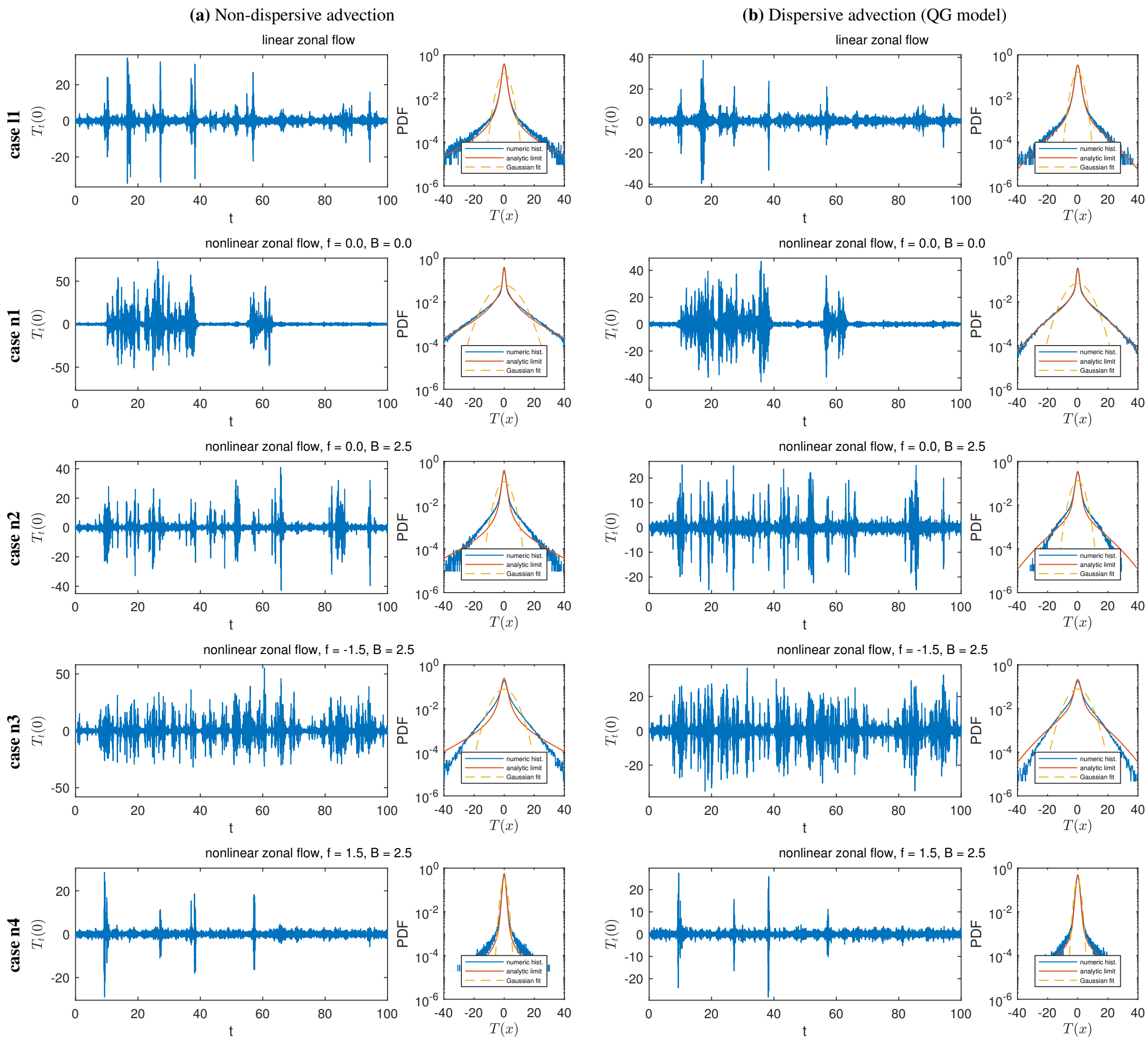

Figure B.12 Comparison of evolution of the tracer field at $T_t(0)$ and the stationary PDF, among different shear flow models.

zonal flow set 2: $\overline{u_r} = 1.6194, \quad \overline{u} = 1.0, \quad c = -0.6194$

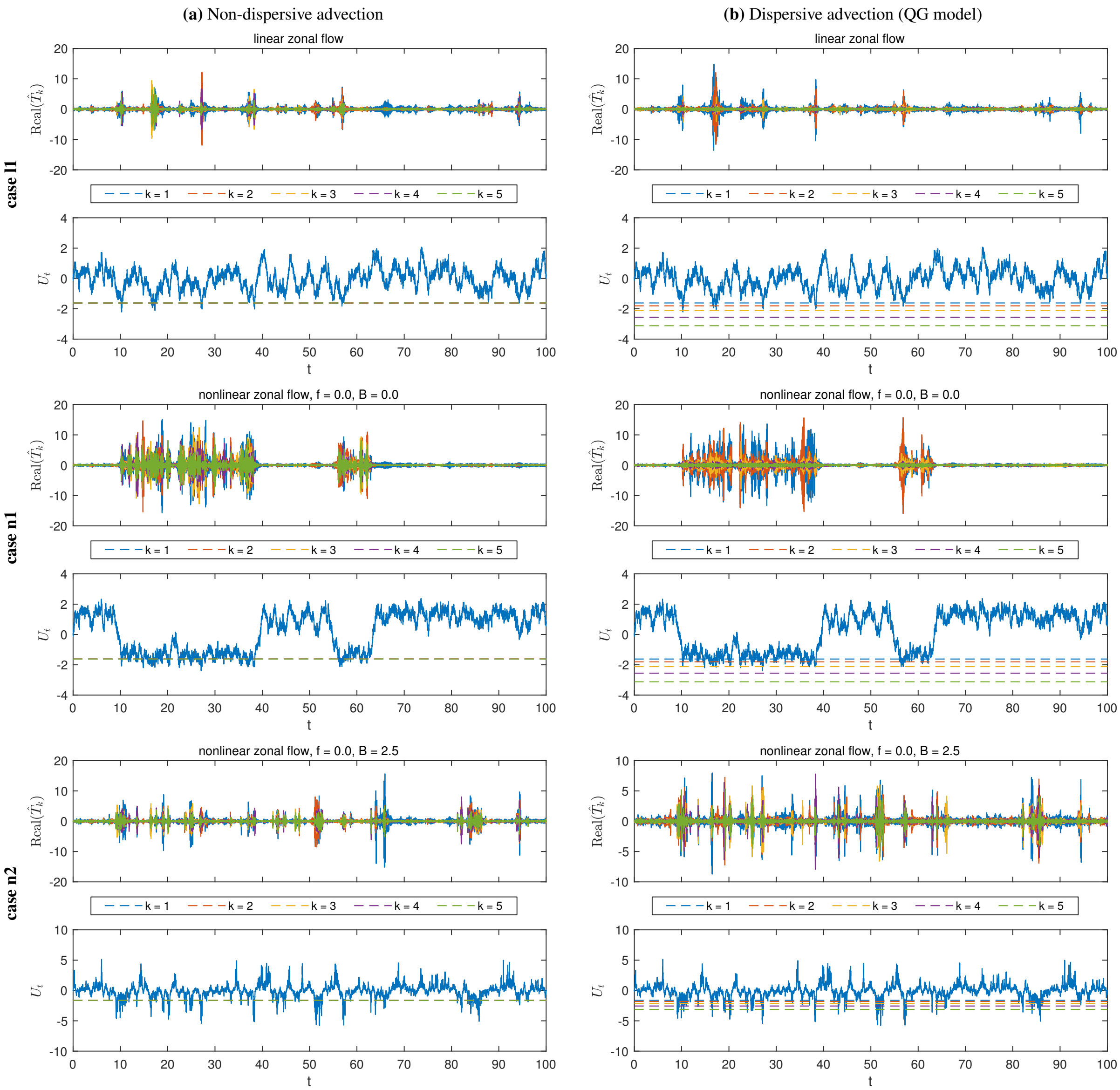

Figure B.13 Comparison of evolution of the tracer modes and zonal fluctuation.